Author Manuscript

Author Manuscript

Author Manuscript

Author Manuscript

HHS Public Access

Author manuscript

Cell Rep. Author manuscript; available in PMC 2021 June 14.

Published in final edited form as:

Cell Rep. 2021 May 25; 35(8): 109157. doi:10.1016/j.celrep.2021.109157.

A systematic analysis of signaling reactivation and drug resistance

Boris N. Kholodenko[1,2,3,4,*], **Nora Rauch**[1], **Walter Kolch**[1,2], **Oleksii S. Rukhlenko**[1]

[1]Systems Biology Ireland, School of Medicine and Medical Science, University College Dublin, Dublin, Ireland [2]Conway Institute of Biomolecular & Biomedical Research, University College Dublin, Dublin, Ireland [3]Department of Pharmacology, Yale University School of Medicine, New Haven, CT, USA [4]Lead contact

SUMMARY

Increasing evidence suggests that the reactivation of initially inhibited signaling pathways causes drug resistance. Here, we analyze how network topologies affect signaling responses to drug treatment. Network-dependent drug resistance is commonly attributed to negative and positive feedback loops. However, feedback loops by themselves cannot completely reactivate steady-state signaling. Newly synthesized negative feedback regulators can induce a transient overshoot but cannot fully restore output signaling. Complete signaling reactivation can only occur when at least two routes, an activating and inhibitory, connect an inhibited upstream protein to a downstream output. Irrespective of the network topology, drug-induced overexpression or increase in target dimerization can restore or even paradoxically increase downstream pathway activity. Kinase dimerization cooperates with inhibitor-mediated alleviation of negative feedback. Our findings inform drug development by considering network context and optimizing the design drug combinations. As an example, we predict and experimentally confirm specific combinations of RAF inhibitors that block mutant NRAS signaling.

Graphical Abstract

This is an open access article under the CC BY-NC-ND license (http://creativecommons.org/licenses/by-nc-nd/4.0/).

*Correspondence: boris.kholodenko@ucd.ie.

AUTHOR CONTRIBUTIONS

B.N.K. and O.S.R. conceived the study. W.K., O.S.R., and B.N.K. wrote the manuscript. B.N.K. and O.S.R. derived the equations and computational models. N.R. performed the experiments.

SUPPLEMENTAL INFORMATION

Supplemental information can be found online at https://doi.org/10.1016/j.celrep.2021.109157.

DECLARATION OF INTERESTS

O.R., W.K., and B.K. filed a patent application (WO2019224216A1) on inhibitor combinations to inhibit kinases whose activation includes dimerization or oligomerization.

Author Manuscript Author Manuscript Author Manuscript Author Manuscript

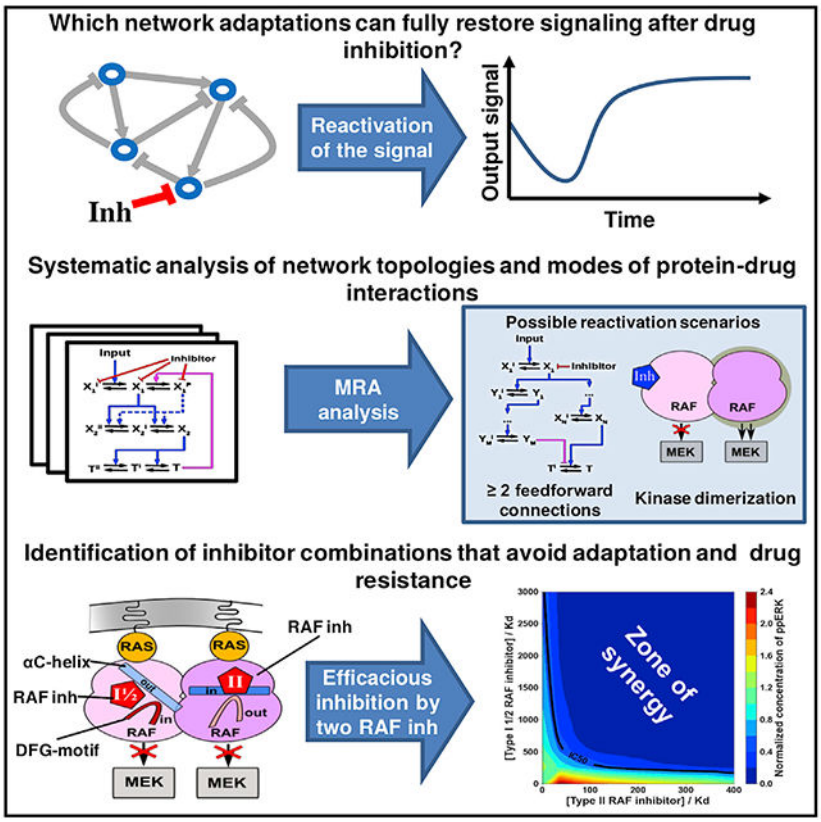

In brief

Kholodenko et al. uncover signaling network circuitries and molecular mechanisms necessary and sufficient for complete reactivation or overshoot of steady-state signaling after kinase inhibitor treatment. The two means to revive signaling output fully are through network topology or reactivation of the kinase activity of the primary drug target. Blocking RAF dimer activity by a combination of type I½ and type II RAF inhibitors efficiently blocks mutant NRAS-driven ERK signaling.

INTRODUCTION

Intrinsic and acquired drug resistances are major clinical problems that limit cancer therapies by targeted drugs. Cancer cell proliferation and survival critically depend on mutated proteins, such as receptor tyrosine kinases (RTKs) or cytoplasmic kinases. This dependence, called oncogene addiction, remains a main concept underlying the rationale to target amplified or mutated oncoproteins for cancer treatment (Weinstein and Joe, 2008). Monoclonal antibody or small-molecule inhibitors are used to target mutated or overexpressed oncoproteins (e.g., ErbB1 in lung cancer, ErbB2 in breast cancer, $BRAF^{V600E}$ mutant in melanoma). Unfortunately, many patients are intrinsically resistant to targeted treatments, whereas other patients, who initially respond, often relapse due to signaling pathway reactivation.

Author Manuscript Author Manuscript Author Manuscript Author Manuscript

Multiple mechanisms of resistance are known, ranging from genetic mutations that abrogate drug binding to network-mediated drug resistance (Kolch et al., 2015; Niederst and Engelman, 2013; Pao et al., 2005). Reactivation of proliferative signals often depends on secondary mutations or amplification of signaling proteins downstream of a primary drug target (Johnson et al., 2015). Alternative, but not mutually exclusive, mechanisms of drug resistance include network adaptations leading to pathways crosstalk, activation of feedback mechanisms, and bypass signaling (Ercan et al., 2012; Lito et al., 2012; Nguyen and Kholodenko, 2016). A surprising mechanism of RAS/RAF/MEK/ERK pathway activation by RAF inhibitors, called paradoxical activation, is due to inhibitor-induced increases in RAF kinase dimerization and subsequent activation (Hatzivassiliou et al., 2010; Heidorn et al., 2010; Kholodenko, 2015; Poulikakos et al., 2010).

Negative and positive feedback loops are ubiquitous in signal transduction. For instance, in the RAS/RAF/MEK/ERK (mitogen-activated protein kinase [MAPK]) cascade, a negative feedback from ERK to RAF is mediated by the inhibitory phosphorylation of RAF kinases (Ritt et al., 2010). Feedback loops mediated by posttranslational modifications (PTMs), such as (de)phosphorylation, operate on a timescale of minutes or tens of minutes. Other types of feedback loops involve the expression of downstream signaling regulators (Amit et al., 2007; Junttila et al., 2008; Nakakuki et al., 2010). Feedback loops involving transcription or translation operate on timescales of hours and days, as reported for growth factor signaling (Mina et al., 2015; Segatto et al., 2011). Negative feedback loops have been implicated as critical mediators in the development of acquired resistance (Chandarlapaty et al., 2011; Sun and Bernards, 2014). However, it remains unclear whether partial or complete, transient, or steady-state reactivation of signaling will occur and how the revival of pathway activity depends on signaling network topology and feedback mechanisms.

Here, we show that negative and positive feedback loops induced by PTMs or transcription/translation are not sufficient, by themselves, for complete reactivation of steady-state pathway signaling following drug inhibition. We also demonstrate that integral feedback, which enables perfect adaptation in engineered bacterial systems (Aoki et al., 2019), cannot fully restore the activity of mammalian signaling systems after drug perturbation of certain network constituents. Systematically analyzing regulatory mechanisms that lead to complete pathway reactivation or overshoot, we identify network topologies that can mediate full pathway reactivation in response to drug inhibition. We demonstrate that two or more feedforward connection routes from an inhibited upstream protein to a pathway output protein are required for full reactivation or increase of the steady-state pathway activity within a range of inhibitor doses. Reactivation is further modulated by kinase dimerization. If the relief of negative feedback by a drug increases the drug-induced kinase dimerization, then this feedback enlarges the range of paradoxical activation. If the drug does not induce dimerization, then the relief of negative feedback only allows a transient overshoot of pathway activity. In the absence of at least two feedforward routes to the output protein, negative feedback regulators can only induce a transient overshoot of the output signaling that has existed before drug treatment, rather than being able to enhance the steady-state output activity. These insights may have profound implications for designing approaches to overcome drug resistance.

Author Manuscript Author Manuscript Author Manuscript Author Manuscript

RESULTS

A need for a systematic network analysis of pathway inhibition and reactivation in response to drugs

Much of drug resistance research has focused on mutations in the target protein(s) that interfere with drug binding and mechanisms that eliminate drugs from the target cells (Aleksakhina et al., 2019; Nikolaou et al., 2018). However, network adaptations emerge as another important source of drug resistance (Klinger et al., 2013). In particular, recent lessons learned from the responses of the RAS/RAF/MEK/ERK pathway to inhibitors have unearthed surprises, such as inhibitors actually activating the pathway (so-called paradoxical activation) (Lee et al., 2020; Rauch et al., 2016). Numerous publications suggest that pathway reactivation due to negative feedback circuits is a key mechanism of resistance to RAF, MEK, $KRAS^{G12C}$ and phosphatidylinositol 3-kinase (PI3K) inhibitors (Lito et al., 2012; Montero-Conde et al., 2013; Prahallad et al., 2012; Ryan et al., 2020; Sun et al., 2014; Yaeger and Corcoran, 2019). To systematically analyze network-mediated adaptations to drug inhibition and pathway re-activation, we have exploited a systems theory, modular response analysis (MRA), and mechanistic modeling of signaling pathways. MRA is based on principles from physics, chemistry, and control engineering, allowing us to analyze and quantify the dynamic responses of different network topologies to drug interference (Kholodenko et al., 2002). Figure 1 illustrates how the MRA-quantified network topology and the local response of the primary target to a drug determine the systems-level drug response (STAR Methods). The topology is given by the connections between network nodes and their strengths. In the MRA framework, network nodes can be single proteins, genes, or entire signaling pathways considered to be modules with defined output species (Halasz et al., 2016; Yalamanchili et al., 2006). The local response of the primary target depends on the mechanisms of drug-target interactions, which can facilitate protein dimerization or change target abundance by changing the synthesis or degradation rates. On a high level, MRA analysis demonstrates that there are only two major means of complete, steady-state revival of signaling, enabled by (1) the network topology or (2) mechanisms rendering the primary target active again. Here, we analyze these statements in detail and dissect the contributions of different feedback and feedforward loops into drug resistance.

Can feedback circuitry reactivate signaling?

Negative feedback occurs when a downstream pathway protein, the signaling output, inhibits an upstream protein, the pathway input. As a result, the output activity directly correlates with the inhibition of the input. A strong input increases both the output and negative feedback that subsequently inhibits the input as self-regulatory loop. This mechanism is commonly held responsible for mediating resistance to drugs that inhibit the input and concomitantly, the negative feedback, allowing recovery of the output. Although intuitively persuasive, it raises a critical question. If a drug inhibits the input, can the steady-state output activity completely recover because of a particular circuitry of feedback loops, which are mediated by either PTMs or expression of negative regulators?

We consider a signaling pathway consisting of layers of PTM cycles, where at each tier, a kinase is phosphorylated and activated by an active kinase of the preceding layer and

Author Manuscript Author Manuscript Author Manuscript Author Manuscript

dephosphorylated by a phosphatase at the same layer (Figure 2A). The first-tier kinase is activated by an external signal, which is considered constant for simplicity. The terminal kinase is the pathway output that inhibits the first-tier kinase. This pathway architecture is similar to the topology of MAPK cascades, which are evolutionarily conserved from yeast to mammals (Widmann et al., 1999)

Pathway response to the inhibition of the first-tier kinase

To understand how the pathway output (T) responds to a drug that inhibits the input kinase X_1, we quantify this response in terms of a systems-level change in T brought about by a small change in the drug dose (I), assuming that the entire pathway relaxes to a stable steady state (Kholodenko et al., 1997),

$$R_{TI} = \left.\frac{dT}{dI}\right|_{\text{system steady state}}. \quad \text{(Equation 1)}$$

This systems-level response R_{TI} is also known as the global pathway response (Bruggeman et al., 2002). Now, for a moment, we consider the first tier, a kinase and a phosphatase, as being isolated from the rest of the pathway. Given the drug I inhibits the kinase X_1, and only this first cascade tier is allowed to relax to its steady state, we quantify the local response ($r_{X_1 I}$) of the primary drug target X_1, as follows,

$$r_{X_1 I} = \left.\frac{\partial X_1}{\partial I}\right|_{\text{first tier steady state}}. \quad \text{(Equation 2)}$$

The kinase X_1 is inhibited by negative feedback from the output protein T, which in turn is activated by X_1 through cascade interactions (Figure 2A). Consequently, the systems-level response R_{TI} will be different from the local response $r_{X_1 I}$. We quantify the negative feedback in terms of the local response ($r_{X_1 T}$) of the first-tier kinase X_1 to its inhibition by T,

$$r_{X_1 T} = \left.\frac{\partial X_1}{\partial T}\right|_{\text{first tier steady state}}. \quad \text{(Equation 3)}$$

To describe how the signal propagates through the cascade, we introduce the local responses ($r_{X_j X_{j-1}}$) of the kinase X_j of tier j to the preceding kinase X_{j-1}, again assuming that only tier j, isolated from the system, relaxes to its steady state,

$$r_{X_j X_{j-1}} = \left.\frac{\partial X_j}{\partial X_{j-1}}\right|_{\text{tier } j \text{ steady state}}. \quad \text{(Equation 4)}$$

The local responses ($r_{X_j X_{j-1}}, r_{X_1 T}$) are also referred to as connection coefficients, because they)quantify the strengths of direct connections between network nodes (Bastiaens et al., 2015; Kholodenko, 2007; Thomaseth et al., 2018). The connection coefficients $r_{X_j X_{j-1}}$ are positive because each kinase is activated by its immediately preceding kinase.

Author Manuscript Author Manuscript Author Manuscript Author Manuscript

We now determine the systems-level response to a drug using the local drug response and the connection coefficients for a given network structure (STAR Methods),

$$R_{TI} = \frac{r_{X_1 I} \cdot P}{1 - r_{X_1 T} \cdot P}; P = r_{X_2 X_1} \cdot r_{X_3 X_2} \ldots \cdot r_{T X_N} > 0. \quad \text{(Equation 5)}$$

The coefficient $r_{X_1 I}$ is negative because the kinase X_1 is inhibited by the drug, and $r_{X_1 T}$ is also negative because the output T inhibits X_1. Therefore, R_{TI} is negative, and its absolute value is always smaller than the absolute value of the local (isolated) response $r_{X_1 I}$ of the primary drug target. In other words, the systems-level response to a drug is attenuated by negative feedback. If the cascade is ultrasensitive (i.e., $P > 1$) (Brown et al., 1997; Ferrell, 1997), then the inhibition of output signaling can be markedly reduced compared to the inhibition of the isolated primary drug target. However, the systems-level signaling response to an inhibitor is always negative and cannot change its sign, meaning that although the inhibition relieves negative feedback, the steady-state output activity cannot be completely restored. This conclusion questions the common explanation that loss of negative feedback restores output signaling and causes drug resistance. Whereas in engineering it is known that proportional negative feedback cannot perfectly restore the systems output, the role of negative feedback in drug resistance was a major misconception due to a multitude of ways how negative feedback can be implemented in biochemical networks.

To illustrate this general conclusion, we built a mass-action kinetic model of a generic three-tier kinase-phosphatase cascade, which resembles a three-tier MAPK pathway (e.g., RAF/MEK/ERK), featuring two-site phosphorylation of kinases X_2 (MEK) and T (ERK) (Figure 2B) (Qiao et al., 2007). This model describes elementary enzymatic steps of every reaction and inhibition of the upstream kinase X_1 (RAF) by the output protein T (STAR Methods). We consider two mechanistic scenarios in which the feedback-mediated modification either does or does not affect the affinity of the feedback-modified form (X_1^P) for the drug (Figure 2C). Red, green, and blue lines show dose responses for a strong feedback, the decreased feedback strength, and in the absence of feedback. Dashed red and green lines correspond to the reduced drug affinity of the feedback-modified primary target. For any mechanistic scenario, signaling reactivation increases as the negative feedback strength increases, but never results in complete reactivation of the output at steady state (Figures 2C). The time course of systems-level drug response shows the initial cascade inhibition, followed by partial reactivation (Figure 2D). When the negative feedback becomes too strong, the system loses stability and sustained oscillations appear (Figure 2E), brought about by the inherent delay in the reaction chain from the upstream kinase X_1 to the pathway output T (Kholodenko, 2000).

Some RAF inhibitors not only block RAF catalytic activity but they also sequester BRAF in an inactive complex with its substrate MEK (Haling et al., 2014). Thus, we also consider this type of inhibition. If the output protein T inhibits the upstream kinase X_1 by sequestration into an inactive complex rather than by inhibitory modification of X_1 (Figure 2F), then the complex concentration, X_1-T, appears in the moiety conservation equations for both X_1 and T (Kholodenko and Westerhoff, 1995). Therefore, a change in the drug dose will influence

Author Manuscript Author Manuscript Author Manuscript Author Manuscript

both active forms, X_1 and T, through the drug-induced change in the X_1-T complex (Figure 2F; STAR Methods). Thus, T will respond to a drug whose primary target is X_1 even when all of the other cascade kinases remain fixed, because X_1 and T are linked through the moiety conservation law. However, the systems-level drug response will still be negative for any drug dose (STAR Methods). Although Equation 5 requires a modification when the negative feedback is mediated by protein sequestration (Lill et al., 2019), the complete revival or overshoot of output signaling cannot occur (Figure 2G).

The logic behind a general statement that the inhibition of negative feedback by itself cannot lead to complete signaling reactivation is straightforward. In signal transduction networks, negative feedback that inhibits the input kinase X_1 has a physical manifestation as a PTM or the formation of the inactive complex. A drug that inhibits X_1 will diminish X_1 activity and consequently the output T and negative feedback to X_1. Let us assume that for a given mechanism of feedback modification and its influence on the drug binding, the decrease in negative feedback inhibition of X_1 is greater than the increase in X_1 inhibition caused by the increased drug dose. Then, the X_1 activity and therefore the output activity T would increase. However, the higher T activity would lead to the higher level of X_1 inhibition, resulting in the decrease rather than the increase in the steady-state X_1 activity. This contradicts our initial assumption that the increase in the drug dose would increase the X_1 activity due to relief in negative feedback.

If a drug affects an intermediate kinase, located within the negative feedback loop (Figure S1A), then the drug effect is buffered, becoming much smaller than the response to a drug that inhibits a top-level kinase (STAR Methods). An example is the RAF/MEK/ERK pathway. Here, negative feedback from ERK to RAF buffers the inhibition of MEK and attenuates the inhibition of the output kinase ERK (Sturm et al., 2010). Simulations of a mechanistic, mass-action model of a three-tiered kinase-phosphatase pathway support these conclusions (Figures S1B and S1C).

To summarize, we stipulate that the inhibition of a negative feedback loop mediated by PTMs or sequestration of the active species cannot completely reactivate steady-state signaling in a kinase pathway. Inhibiting a target embedded within a negative feedback loop is less effective than inhibition of an upstream target.

A cascade with several feedback loops—Most cellular signal transduction networks are regulated by intertwined negative and positive feedback loops. We show that no combination of feedbacks coming from the pathway output or from an intermediate kinase can ensure a complete recovery of signaling output. As an example, we consider a pathway in which two feedbacks, negative and positive, arise from the output protein T and affect the upstream kinase X_1 (Figure 2H). These feedback loops can occur as PTM-mediated interactions within the same pathway, or they can go through different intermediates of other pathways (Y and Z), as shown in Figure 2H. Given that one feedback (e.g., through Y) is positive and the other (through Z) is negative, the local response of the activity of the kinase X_1 to changes in T will be positive for the Y loop ($r_{X_1Y} \cdot r_{YT} > 0$) and negative for the Z loop ($r_{X_1Z} \cdot r_{ZT} < 0$). A positive feedback ($Y$ loop) can be carried out by two consequent

Author Manuscript Author Manuscript Author Manuscript Author Manuscript

negative feedbacks or two positive feedbacks, so that the product $r_{X_1Z} \cdot r_{ZT} > 0$ in either case. The systems-level response (R_{TI}) of the output T to drug I is expressed in terms of the connection coefficients (local feedback responses) and the product P of the activating connections along the pathway (STAR Methods),

$$R_{TI} = \frac{r_{X_1I} \cdot P}{1 - \left(r_{X_1Y} \cdot r_{YT} + r_{X_1Z} \cdot r_{ZT}\right)P} \qquad \text{(Equation 6)}$$
$$P = r_{X_2X_1} \cdot r_{X_3X_2} \cdots \cdot r_{TX_{N-1}} \cdot$$

Because of a combination of negative and positive feedback terms ($r_{X_1Z} \cdot r_{ZT} < 0$, $r_{X_1Y} \cdot r_{YT} > 0$), the denominator of Equation 6 is >1, if the negative feedback arm prevails. In this case, drug inhibition is attenuated. If the positive feedback prevails, then the denominator becomes <1, and the drug effect is amplified. At first glance, a further increase in the positive feedback strength could make the denominator negative, changing the sign of the drug response to positive, meaning that the inhibitor would increase the output activity. However, when the denominator passes through zero, the steady state loses stability, and an additional unstable state emerges in a so-called saddle-node bifurcation (Kholodenko, 2006; Kuznetsov, 2004). The pathway response R_{TI} to the inhibitor is positive only for this unstable state. Therefore, a combination of positive and negative feedback loops cannot restore the pathway activity to the level observed before inhibitor treatment.

Transient pathway reactivation by expression of negative feedback regulators—In addition to immediate, PTM-mediated regulatory connections, signaling pathways are controlled by feedback circuitries that initiate the expression of feedback regulators (Amit et al., 2007; Boutros et al., 2008; Jones et al., 2018; Mukherjee et al., 2021). For the sake of brevity, we call these transcriptional loops. The stable steady-state behaviors of networks with the same connection topologies are similar for both PTM-mediated and transcriptional regulatory connections. Therefore, the above conclusions about network topologies and features that bring about paradoxical pathway activation by inhibitors continue to apply to networks that involve transcriptional feedback loops. However, there are essential distinctions between the rapid regulation by PTMs and the control by transcriptional loops. Transcriptional feedback and feedforward loops involve processes that occur on timescales that are orders of magnitude longer than (de)phosphorylation events. Delays in transcriptional feedback circuits can lead to sustained oscillations, such as circadian rhythms (Aronson et al., 1994; Feillet et al., 2015; Goldbeter, 1995), whereas a steady state of a pathway with the same topology of (de)phosphorylation connections can be stable. Even when stable steady-state behaviors are similar, the temporal patterns of responses to perturbations, such as drug treatments, will be different for networks with solely PTM-mediated regulations or those that involve transcriptional connections. The network response time to drug perturbations may be so long that even before transcriptional loops reach the steady state, cell fate decisions would be made based on transient signaling responses (Volinsky and Kholodenko, 2013).

Growth factor signaling induces the expression of multiple negative feedback regulators operating at different signaling layers, from RTKs to downstream kinases, such as the

Author Manuscript Author Manuscript Author Manuscript Author Manuscript

MAPK family. For instance, the MAP kinases JNK, p38, and ERK activate transcription of dual-specificity phosphatases (DUSPs), which can dephosphorylate the cognate MAPK that induced this DUSP, as well as other MAPKs, leading to crosstalk between different MAPK pathways (Caunt and Keyse, 2013; Junttila et al., 2008). Other negative feedback regulators of growth factor signaling include ERK-induced expression of the ERBB receptor feedback inhibitor 1 (also known as MIG-6, ERRFI1, or RALT), which is a potent inhibitor of epidermal growth factor receptor (EGFR), ERBB2, and ERBB4 (Milewska et al., 2015), and the SPRY domain-containing proteins (e.g., SPRY-2), which bind to and inhibit receptors and several other upstream proteins, such as GRB2 and CBL (Frank et al., 2009; Wong et al., 2002).

We next examined the dynamics of the JNK pathway that embraces phosphorylation-mediated positive feedback loops and transcriptional negative feedback (Figure 3A). JNK phosphorylates and activates the immediately preceding kinase MKK4 in neuroblastoma cells, and activates an upstream MAPKKK (e.g., MLK, ASK) in other cell types (Fey et al., 2015; Ventura et al., 2006). In addition, JNK induces the expression of its phosphatase, DUSP1 (Ventura et al., 2006). Inhibition of JNK or its upstream kinase is amplified by rapid positive feedback and initially strongly suppresses JNK signaling (Figures 3A and 3B). This reduced JNK activity decreases mRNA synthesis and expression of DUSP1, which leads to slow reactivation, followed by the overshoot of JNK activity on the timescale of hours. However, complete reactivation of steady-state JNK signaling cannot occur (Equation 6). Thus, the large delay in the transcriptional negative feedback circuits is a key distinction from the rapid PTM-mediated regulation. If the system is stable, then an increase in the delay time often results in the appearance of the activity overshoot before the output activity approaches the steady state, as illustrated in Figure 3B. The delays in negative feedback loops combined with sensitivity amplification are common mechanisms of damped or sustained oscillatory responses of signaling cascades to perturbations (Dibrov et al., 1982; Kholodenko, 2000; Tyson and Othmer, 1978).

The integral feedback control—When the degradation time of *de novo* synthesized regulators is much greater than the timescale of the network evolution regulated by the PTM-mediated control circuitry, signaling network dynamics are often described using the integral feedback control (Goyal et al., 2017; Nakakuki et al., 2010). The integral feedback control is widely used in industrial process control applications (Bennett, 1996). In this strategy, the time integral of the difference between the current output of a system and its preper-turbation level, which is called the error, feeds back to regulate the system output. A hallmark of integral controllers is the complete elimination of the steady-state error, leading to complete or perfect adaptation to noise and other disturbances. However, when the effect feedback regulator on the signaling output is described by the integral control, a system cannot reach a true steady state because the abundance of *de novo* synthesized regulators increases indefinitely, while the abundances of other network constituents remain constant (STAR Methods).

Integral feedback can ensure perfect adaptation (Yi et al., 2000). A marked difference between the transcriptional regulation of upstream signaling and the integral feedback is that integral feedback depends not only on the current network state but also on the previous

Author Manuscript Author Manuscript Author Manuscript Author Manuscript

states. A synthetic transcriptional network, in which so-called antithetic integral feedback is compatible with steady-state requirements has recently been described (Aoki et al., 2019). Its key property is the presence of at least two *de novo* synthesized controlling species. One of these species must be synthesized at a constant rate to activate the regulated network. The synthesis of the second controlling species is induced by the output of the regulated network. The other necessary feature is an annihilation reaction, in which these two species or their derivatives form a mutually inhibitory complex that subsequently degrades. Although this design is based on a proven mathematical theorem, its main assumption fails for cell signaling networks, if the moieties of interconverted protein forms are conserved at the time of observation. In STAR Methods, we provide rigorous proof that for an arbitrary signaling network, in which the total abundance of different forms of the primary drug target or other proteins that transfer the signal are conserved (Figures S2A and S2B), antithetic integral feedback cannot result in complete reactivation of signaling. We also illustrate this proof in STAR Methods, using realistic examples of signaling networks (Figures 3D–3H and S2C–S2E).

To summarize, negative transcriptional regulators can lead to slow reactivation and overshoot of output signaling following initial pathway inhibition. However, when the steady-state activity is finally reached, the signaling output will normally be below the original level. Mammalian signaling systems with integral feedback cannot completely restore the original signaling output after the inhibition of many primary drug targets, because moiety conservation of interconverted protein forms is the rule rather than an exception. We conclude that for complete and robust reactivation following a drug inhibition, a signaling network must have additional features, other than positive and/or negative feedback loops.

Complete reactivation or overshooting of the pathway output activity

Motivated by the conclusion that feedback loops alone cannot fully reactivate pathways after drug inhibition, we have analyzed potential complementary mechanisms. We show that complete reactivation of steady-state signaling following drug treatment can emerge if a network involves (1) feedforward connections from the primary drug targets to signaling output, (2) pathway crosstalk, or (3) when the inhibitor triggers paradoxical pathway activation by inducing dimerization/oligomerization and concomitant activation of its direct target (Koppikar et al., 2012). Negative and positive feedback loops merely modulate reactivation of the signaling output and, depending on the pathway topology and allosteric inhibitor-target interactions, may amplify or attenuate drug resistance.

Signaling reactivation brought about by pathway crosstalk—Complete reactivation or overshoot of steady-state signaling can emerge for a range of drug doses, if there are two or more connection routes from the upstream primary drug target to the downstream output. For topological reasons, these routes cannot be formed only by feedback loops. An additional feedforward connection to the output protein is necessary, which can exist, for instance, as crosstalk between two pathways.

Author Manuscript Author Manuscript Author Manuscript Author Manuscript

In a typical crosstalk, an upstream kinase signals to an output protein through a kinase cascade, but also directly or indirectly activates another pathway that inhibits this output protein (Figure 4A). This topology is known as a negative or incoherent feedforward loop (Mangan and Alon, 2003). A similar topology is found in tumor cells with mutant RAS that activates both the RAF/MEK/ERK cascade and the p38 pathway, which in turn can inhibit ERK (Figure 4B) (Fey et al., 2012).

The pathways X and Y converge onto the same signaling output (Figure 4A). We denote the products of the connectivity coefficients along each pathway to the shared output T as P_X and P_Y, respectively,

$$P_X = r_{X_2X_1} \cdot \ldots \cdot r_{TX_{N-1}} > 0; P_Y = r_{Y_1X_1} \cdot r_{Y_2Y_1} \ldots \cdot r_{TY_M} < 0$$

Because kinases in the pathway X activate each other and subsequently the output T, the P_X value is positive. At the same time, P_Y is negative, because the pathway Y inhibits T. For instance, T can be inhibited by the kinase $Y_M\left(r_{TY_M} < 0\right)$, whereas Y_M is activated by the reaction chain $Y\left(r_{Y_1X_1} > 0, r_{Y_2Y_1} > 0, \ldots, r_{Y_MY_{M-1}} > 0\right)$ (Figure 4A). P_X or P_Y shows how sensitive the output is to the changes in the upstream kinase activity X_1 when the signal propagates only through the pathway X or the pathway Y.

Given the primary drug target is the upstream kinase X_1, the systems-level response (R_{TI}) to the drug I equals the local response ($r_{X_1I} < 0$) of the kinase X_1 to this drug, multiplied by the sum (P_X and P_Y) of the products of the connectivity coefficients along each pathway (STAR Methods),

$$R_{TI} = r_{X_1I} \cdot (P_X + P_Y). \quad \text{(Equation 7)}$$

Depending on the connection strengths that determine the sensitivity of the output to signals propagating through each pathway, the sum ($P_X + P_Y$) can be positive or negative. Moreover, with the change in the inhibitor dose and the resulting change in the upstream kinase activity, the sign of the sum ($P_X + P_Y$) can change.

If at low drug doses the negative sensitivity P_Y prevails, then the sum ($P_X + P_Y$) is negative. Because the upstream kinase is inhibited, its local response is also negative, $r_{X_1I} < 0$. The product of these two values (i.e., the systems-level response R_{TI} in Equation 7), will be positive. This means that output signaling will be activated by low doses of a drug that inhibits the input kinase X_1 (Figure 4C). The dose range for this “paradoxical activation” depends on the network kinetics. Initially, pathway activation increases with drug dose, but at large doses both pathways and their common output eventually will be inhibited (Figure 4C). If the positive sensitivity P_X prevails at low inhibitor doses, then the sum ($P_X + P_Y$) is positive. Consequently, R_{TI} will be negative, so the signaling output will be inhibited by the drug at low inhibitor doses. With increasing inhibitor doses and a decrease in the kinase X_1 activity, the negative sensitivity can become dominant, and the sum ($P_X + P_Y$) turns negative. As a result, the systems-level response R_{TI} will become positive, and within a

Author Manuscript Author Manuscript Author Manuscript Author Manuscript

range of inhibitor doses, the signaling output becomes paradoxically activated by the inhibitor (Figure 4D).

If pathway crosstalk occurs downstream of the kinase X_1, paradoxical activation of the output T can occur when the drug inhibits a kinase that is located upstream of negative feedforward connection to T (Figures S3A and S3B), but not by inhibition of a kinase within the feedforward loop or the output kinase itself (Figures S3C and S3D; STAR Methods). Clearly, the inhibition of the pathway Y only can activate the output. Thus, the key element of reactivation and overshoot of the output activity via crosstalk is the interplay between positive and negative signals that propagate from the primary drug target to the downstream output.

Modulation of paradoxical inhibitor responses emerging from pathway crosstalk by feedback loops—Whereas feedforward connections are necessary for the activation of the pathway output by an inhibitor, feedback loops will modulate the extent of paradoxical activation and the range of drug doses where it occurs.

If the output feeds back to the upstream kinase at the crosstalk point (Figure 4E), then the output responses propagate to both pathways. Additional interaction points can be created by feedback loops between intermediate kinases of two pathways. The systems-level response (R_{TI}) of the shared output to a drug (I) is expressed in terms of the local kinase response ($r_{X_1 I} < 0$), the products (P_X and P_Y) of the connectivity coefficients along the cross-talking pathways, and the feedback connection strength ($r_{X_1 T}$) (see STAR Methods),

$$R_{TI} = \frac{r_{X_1 1} \cdot (P_X + P_Y)}{1 - r_{X_1 T} \cdot (P_X + P_Y)}. \quad \text{(Equation 8)}$$

This response resembles the response of a single pathway with feedback (Equation 5), but here feedback integrates the responses along two pathways. Because negative feedback attenuates the drug inhibition, it will also narrow the range of drug doses where signaling is reactivated via pathway crosstalk. Positive feedback amplifies the drug action, and it will enlarge the range of paradoxical activation by an inhibitor. Figures 4F and 4G illustrate this modulation of responses.

If the primary drug target is localized upstream of the crosstalk point but inside a feedback loop (Figures S3E–S3G), then complete reactivation of output signaling still occurs for a range of drug doses. However, if a drug inhibits a kinase located downstream of the crosstalk point (Figures S3H–S3J), the systems-level response to this inhibitor will always be negative, ruling out paradoxical activation of the pathway (STAR Methods).

Notwithstanding the integration by feedback, at least two feedforward routes from the primary drug target to the output that include positive and negative connections are necessary to observe paradoxical inhibitor responses. A route can embrace feedback loops, but the direction of signal propagation to the output is feedforward (Figures S4A and S4B). A mathematical formulation is given in STAR Methods together with a method to obtain the number of routes connecting the primary drug target with the network output. Figures S4C

Author Manuscript Author Manuscript Author Manuscript Author Manuscript

and S4D illustrate different dose responses for paradoxical pathway activation by an inhibitor depending on what route is dominant.

Negative and positive feedback loops cannot by themselves fully reactivate pathway signaling following the inhibition of an upstream kinase. Two or more routes need to connect the inhibited kinase to the output protein. These routes can incorporate feedback loops but inevitably require feedforward connections. Negative and positive feedback loops not only propagate the responses of downstream proteins back to the input but also reduce or enlarge the ranges of drug doses in which pathway reactivation is observed, as well as the magnitude of signaling overshoot.

Opposite drug responses emerging at hysteresis branches—Positive or double-negative feedback loops intertwined with descending feedforward routes from a primary drug target can lead to the emergence of switch-like, bistable responses to a drug (Kaimachnikov and Kholodenko, 2009). When the drug dose gradually increases or decreases, a bistable network can switch between two stable but different steady states. A hallmark of bistable systems is hysteresis. In STAR Methods, we show that at different hysteresis branches corresponding to alternative steady states, the drug responses can behave differently. Increasing the drug dose will decrease signaling at one hysteresis branch and increase signaling at the other branch (Figures S5A and S5B). Depending on the history of drug treatment, for the same drug dose the output activity can be high or low, and distinct responses to a drug are observed at different hysteresis branches.

Pathways with multiple output proteins: Inhibition of one output leads to activation of the other and concomitant drug resistance—Signaling pathways, which crosstalk to one another, often have multiple outputs, including shared outputs (Klinger and Blüthgen, 2014). Because of crosstalk and feedforward loops, the inhibition of one output protein may result in the activation of another output. For instance, if there is negative feedback from the first output to a kinase at the crosstalk point or further upstream, then inhibition of this output will reduce the negative feedback influence. Crosstalk between two pathways was suggested as a mechanism of resistance by Zañudo et al. (2018). Figures S5C and S5D illustrate that the inhibition of the output T_1 activates another output T_2 by alleviating the inhibition of T_2. If there are negative and positive feedback loops from T_1 to the upstream kinases (Figure S5E), then its inhibition by a drug results in the activation or inhibition of another output T_2 at a range of drug doses. These dose responses adopt convex or concave shapes depending on the dominant feedback effect in different dose ranges (Figures S5F and S5G).

Kinase dimerization cooperating with negative feedback conveys pathway reactivation and drug resistance

Many bona fide kinase inhibitors increase the activity of their targets, causing paradoxical activation. This effect was first described for RAF inhibitors by Hall-Jackson et al. (1999), and later shown to be related to increased RAF homo- and heterodimerization that is facilitated by RAF inhibitors (Heidorn et al., 2010; Poulikakos et al., 2010). Not only the RAF kinases but also many other kinases are activated by homo- and heterodimerization and

Author Manuscript Author Manuscript Author Manuscript Author Manuscript

oligomerization (Bessman et al., 2014; Dey et al., 2005; Hu et al., 2013; Huang et al., 2014; Wang et al., 2012). Here, we show that negative feedback cooperates with paradoxical activation in the reactivation of a pathway, if the inhibitor-induced alleviation of this feedback increases kinase dimerization (Lito et al., 2012).

Paradoxical activation of the RTK/RAS/RAF/MEK/ERK pathway by RAF inhibitors—Using a previous study (Rukhlenko et al., 2018), we have built a structure-based dynamic model of the RAS/RAF/MEK/ERK pathway that sheds light on the mechanisms of paradoxical RAF activation by RAF inhibitors facilitated by negative feedback loops (see STAR Methods for details). We analyze these mechanisms and dose responses to inhibitors in cells bearing activating $BRAF^{V600E}$ mutation or wild-type (WT) BRAF, and either WT RAS or mutant RAS genes.

In melanoma cells harboring the $BRAF^{V600E}$ mutation and WT RAS, the high $BRAF^{V600E}$ kinase activity induces strong ERK-mediated feedback phosphorylation of SOS on inhibitory residues resulting in suppressed SOS activity and low RAS-guanosine triphosphate (GTP) levels. RAF binding to RAS-GTP is required for RAF dimerization, which greatly increases the RAF kinase activity (Rushworth et al., 2006). Because RAS-GTP is low, $BRAF^{V600E}$ molecules remain monomers with high constitutive activity. RAF inhibitors strongly inhibit $BRAF^{V600E}$ monomers, transiently decreasing MEK and ERK activities (Figure 5B). However, the concomitant decrease in SOS inhibitory phosphorylation increases SOS activity and RAS-GTP levels. In addition, RAF inhibitors allosterically promote RAF dimerization, reducing the apparent dimerization constant (K_d). Together with the enhanced RAS-GTP, the decrease in K_d prompts homo- and heterodimerization of $BRAF^{V600E}$ with WT BRAF and CRAF, leading to inhibitor-induced paradoxical activation of ERK signaling. Our model demonstrates that this induction of RAF dimers brings about complete reactivation and overshooting of the ERK activity (Figure 5B).

Importantly, negative feedback from active ERK to SOS (and also to RTKs) cannot by itself reactivate the pathway or induce its paradoxical activation following RAF inhibitor treatment without RAF dimerization (Figure 5C). The inhibitor-induced RAF dimerization is a necessary prerequisite for ERK reactivation and can bring about paradoxical pathway activation by itself (Kholodenko, 2015). Negative feedback increases the range of RAF inhibitor doses where pathway reactivation is observed, but it can also decrease the peak value of paradoxical activation.

Combining two RAF inhibitors blocks ERK pathway reactivation more effectively than combining RAF and MEK inhibitors in NRAS mutant cells

A combination of RAF and MEK inhibitors can reduce ERK reactivation (Sturm et al., 2010) and is now the standard of care for $BRAF^{V600E}$-driven metastatic melanoma (Grob et al., 2015; Larkin et al., 2014; Lito et al., 2012). Although this inhibitor combination can suppress ERK activity better than a single RAF inhibitor, attenuation of ERK-mediated negative feedback loops to SOS and upstream RTKs can make this combination ineffective, especially at low or moderate RAF inhibitor doses. Currently, three types of RAF inhibitors are available: type I, binding an active RAF conformation with the DFG motif and αC-helix

Author Manuscript Author Manuscript Author Manuscript Author Manuscript

in “IN” positions (DFG-IN/αC-IN); type II, binding the inactive DFG-OUT/αC-IN conformation; and type I½ binding the DFGIN/αC-OUT RAF. Next, we show that whether RAF and MEK inhibitors will or will not exhibit synergy is determined by the type of inhibitors and RAS-GTP levels in WT RAS and RAS mutant cells.

The efficiency of the ERK inhibition by a two-drug combination is comprehensively assessed by determining the ppERK response across a two-dimensional plane of drug doses (Keith et al., 2005; Yeh et al., 2009). Lines of constant inhibition are called Loewe isoboles (Greco et al., 1995). For non-interacting drugs, these isoboles are straight lines. If two inhibitors synergize, then Loewe isoboles are concave, because lesser doses result in the same inhibitory effect, whereas convex isoboles indicate antagonism between inhibitors, because the doses must increase to achieve the same inhibition level.

Using the model, we calculated Loewe isoboles for combinations of a type I½ RAF inhibitor (e.g., dabrafenib or encorafenib) and a MEK inhibitor (trametinib or binimetinib), which are currently used in the clinic. We performed these calculations for different levels of RAS activity based on literature estimates ((Romano et al., 2014); Rukhlenko et al., 2018)— high RAS activity observed in mutant RAS cells (~250 nM RAS-GTP of 750 nM total RAS), low RAS activity (~25 nM RAS-GTP of 750 nM total RAS) as in WT RAS and $BRAF^{V600E}$ cells where RAS activation is feedback inhibited, and medium RAS activity (~100 nM RAS-GTP of 750 nM total RAS) as in cells where WT RAS is feedback inhibited but simultaneously stimulated by RTK overexpression. For WT RAS, $BRAF^{V600E}$ melanoma cells with low RAS activity, our model shows that Loewe isoboles are concave for a wide range of concentrations of these drugs, demonstrating synergy between RAF and MEK inhibitors (Figure 5D). However, this combination can even turn antagonistic when inhibitor concentrations are low and RAS-GTP levels are constitutively high, such as in RAS mutant cells. For instance, a combination of dabrafenib and trametinib showed marked antagonism in MEL-JUSO melanoma cells harboring two oncogenic RAS mutations ($NRAS^{Q61L/WT}$ and $HRAS^{G13D/G13D}$) and WT BRAF (Rukhlenko et al., 2018). This is likely due to a two-pronged mechanism, in which MEK inhibition releases the negative feedback from ERK to RAF, thereby increasing RAF dimerization, while the RAF inhibitor further induces RAF dimerization and activation of RAF signaling to ERK. Elevating RAS-GTP levels in WT RAS, $BRAF^{V600E}$ cancer cells (e.g., by RTK overexpression) shift the Loewe isoboles to the right, showing that higher type I½ RAF inhibitor doses are required to achieve 25% and 50% of ERK inhibition (Figure 5E). At low RAF inhibitor concentrations, the RAF dimerization related to paradoxical activation prevails, causing a small zone of antagonism with MEK inhibitors (Figure 5D). Once that zone is passed, type I½ RAF and MEK inhibitors can synergize over a wide dose range. The synergy is dampened as RAS activity increases (Figure 5E). Moreover, at relatively large doses, a MEK inhibitor may be more effective on its own than in combination with a RAF inhibitor, when the RAF inhibitor is given at doses that are within the range of paradoxical ERK activation (Figure 5E). Because the maximum blood plasma levels for MEK inhibitors are low (Table S2), these doses can be insufficient for achieving the desired therapeutic effects.

For several type II RAF inhibitors, such as LY3009120, AZ-628, TAK-632, TAK-580, or lifirafenib, which have low apparent dissociation constants and a narrow range of

Author Manuscript Author Manuscript Author Manuscript Author Manuscript

paradoxical activation, synergy with MEK inhibitors has been observed (Yen et al., 2018; Yuan et al., 2020). However, our calculations suggest that the zone where antagonism prevails can still be substantial, and sufficiently high doses of type II RAF inhibitors are required to remain in the synergy zone (Figure 6A). This is highlighted in Figure S6A, where the Talalay-Chou combination index (CI) is calculated across ranges of RAF and MEK inhibitor doses. Drug synergy, additivity, or antagonism are observed when the CI is <1, equal to 1, or >1, respectively (Chou, 2010). We see that only at high RAF and MEK inhibitor doses, the CI is substantially smaller than 1, indicating synergy. Maintaining high doses of type II RAF inhibitor continuously is difficult to achieve and may increase drug side effects. For many other RAF inhibitors, which have a wide dose range of paradoxical activation (e.g., type I½ inhibitors such as vemurafenib), reaching a zone of synergy with MEK inhibitors is practically impossible in RAS mutant cancers.

Our model suggests effective ways to counteract reactivation of the ERK pathway induced by RAF dimerization and multiple negative feedback loops from ERK. A combination of types I½ and II RAF inhibitors substantially decreases the dose range of paradoxical activation for both inhibitors and, therefore, in RAS mutant cells, synergizes in ERK inhibition over a wider dose range than a combination of RAF and MEK inhibitors (Figures 6B and S6B). The maximally tolerable plasma blood levels demonstrate that type I½ RAF inhibitor can be given in doses >30 times greater than doses of MEK inhibitors, normalized by their K_d values, thereby having a larger therapeutic window (Table S2).

Experimental validation of model predictions—To verify model predictions, we measured ERK phosphorylation responses to diverse types of RAF and MEK inhibitors in two RAS mutant cell lines, melanoma MEL-JUSO ($NRAS^{Q61L/WT}$, $HRAS^{G13D/G13D}$) and acute myeloid leukemia (AML) OCI-AML-3 ($NRAS^{Q61L/Q61L}$). We tested type I½ (vemurafenib and encorafenib) and type II (TAK-632) RAF inhibitors and different allosteric MEK inhibitors, trametinib and cobimetinib, which bind to the same pocket in MEK but shape it in distinct ways (Khan et al., 2020). To compare different dosages, we normalized the inhibitor concentrations by their K_d. This corrects for different inhibitor affinities and allows a direct comparative evaluation of possible synergistic or antagonistic effects. The doses tested were determined by titrating each inhibitor as described previously (Rukhlenko et al., 2018). The doses shown in Figures 6C–6E correspond to ranges in which paradoxical ERK activation by RAF inhibitors is observed, and to IC_{20} or IC_{40} for MEK inhibitors. This design allows the observation of both synergistic and antagonistic effects, particularly effects on paradoxical ERK activation. Types I, I½, and II RAF inhibitors exhibit paradoxical activation of the ERK pathway, although in different dose ranges (Karoulia et al., 2016). The dose range of paradoxical ERK activation was still noticeable for low doses of the type II RAF inhibitor TAK-632 (Figures 6C, 6D, and S6C). Testing a combination of TAK-632 and trametinib in MEL-JUSO cells, we found that ERK inhibition achieved by trametinib decreased after adding TAK-632 in doses within a zone of paradoxical ERK activation (Figures 6C and S6A). Therefore, this inhibitor combination did not synergize. Unlike trametinib, cobimetinib and a type II RAF inhibitor show synergistic inhibition of ERK signaling (Figure 6D), in line with previous data (Yen et al., 2018). However, replacing cobimetinib by type I½ inhibitors (vemurafenib and encorafenib) for a

Author Manuscript Author Manuscript Author Manuscript Author Manuscript

combination with type II RAF inhibitor resulted in a stronger synergistic effect, further decreasing ERK activity (Figures 6D and S7B), exactly as predicted by the model.

We next tested a combination of cobimetinib and TAK-632 in the NRAS mutant AML cell line, OCI-AML-3. Intriguingly, there was no synergy but rather antagonism between these MEK and type II RAF inhibitors within the range of paradoxical RAF activation (Figure S7C). However, a combination of type I½ (vemurafenib and encorafenib) and type II (TAK-632) synergistically and efficaciously suppressed the ERK pathway activity (Figures 6E and S7C). Thus, experimental results obtained for these cell lines and diverse RAF and MEK inhibitors support our model predictions.

A reason for the observed responses in mutant RAS cells is that a MEK inhibitor can attenuate the negative feedback phosphorylation of CRAF and BRAF by ERK (Sturm et al., 2010), but it is unable to prevent the RAF inhibitor-induced RAF dimerization, which drives ERK activation. The extent of synergy (or lack thereof) depends on which RAF (de)activating inputs are available in a cell (e.g., RTK overexpression or concentration of proteins that regulate RAF dimerization) (Baljuls et al., 2013; Bla ževitš et al., 2016; Boned Del Río et al., 2019). Only two RAF inhibitors with different conformation specificity effectively can inhibit RAF dimers (Kholodenko, 2015). Consistent with this explanation, synergy between type I½ and type II RAF inhibitors was even observed for the dose ranges in which each inhibitor on its own paradoxically activates ERK signaling (Figures 6D and 6E). The decrease in the range of paradoxical activation for a combination of types II and I½ RAF inhibitors helps avoid ERK activation when drug availability decreases because of inhibitor clearance. Thus, although high doses of type II RAF inhibitors synergize with both MEK and RAF inhibitors in NRAS mutant cells, we conclude that a combination of two RAF inhibitors is advantageous, as this combination substantially broadens the zone of synergy and diminishes the zone of antagonism.

The paradoxical response of the primary target to an inhibitor activates output signaling rather than inhibits it. This mechanism is distinct from activation caused by feedbacks. A well-studied paradoxical ERK activation in response to RAF inhibitors is caused by RAS-dependent RAF dimerization, which is facilitated by RAF inhibitors and can cooperate with negative feedback loops from ERK to RTKs, SOS, and RAF kinases. A combination of type I½ and type II RAF inhibitors is highly effective in reducing ERK pathway reactivation that otherwise would lead to drug resistance. The model and experiments suggest that this inhibitor combination can efficiently block ERK activation in cancer cells that steadily maintain high RAS-GTP levels.

DISCUSSION

Our analysis shows that no combination of feedback loops can completely restore the steady-state output activity that existed before the inhibition by a drug. The alleviation of negative feedback by a drug is commonly considered a key factor in drug resistance (Ishii et al., 2013; Montero-Conde et al., 2013; Mukherjee et al., 2021; Prahallad et al., 2012). Our results confirm that feedbacks are important contributors. However, at least two feedforward routes, activating and inhibitory, which emanate from the primary drug and converge at the

Author Manuscript Author Manuscript Author Manuscript Author Manuscript

same output, are necessary for the full revival of signaling after drug treatment (Figure 4). In cancer, the activating route is often provided by crosstalk with other pathways that bypass the drug block (Alexander and Wang, 2015).

Although feedback circuitries by themselves cannot fully reactivate steady-state signaling, intrinsic delays in feedback loops can cause a slow transient reactivation and overshoot above the pre-inhibition level. These time delays are typically due to transcriptionally induced feedback inhibitors, such as DUSPs or SPOUTY/SPRED proteins in the MAPK pathways (Lake et al., 2016). Only integral feedback could lead to perfect adaptation to disturbances. However, the molecular realization of integral feedback control imposes restrictive requirements, which can be achieved in synthetic systems (Aoki et al., 2019) but have not been found in mammalian signaling networks. Consequently, mammalian signaling networks with integral feedback modules cannot fully restore output activities after drug inhibition (Figures 3D, 3G, S2D, and S2E; STAR Methods).

Clearly, drug resistance does not necessarily imply perfect reactivation of signaling. However, when reactivation is incomplete, there will always be a drug dose that produces a desired level of inhibition of its target and the pathway output. If this dose exceeds the therapeutic window, then resistance will prevail, but optimizing drug combinations can improve the pathway inhibition and the total dose of drugs in a combination will be smaller than a dose of a single drug.

Besides network topology-mediated mechanisms, the activity of a primary drug target can be restored by overexpression or mutation of this target, or by increasing its dimerization and subsequent kinase activity. If dimerization induces allosteric activation, drugs that enhance dimerization lead to paradoxical activation of the drug target. If the alleviation of a negative feedback further increases dimerization, then the paradoxical activation of this kinase will increase further. The two common mechanisms of resistance to RAF inhibitors in $BRAF^{V600E}$ melanoma are due to activating mutations in *NRAS* gene or expression of $BRAF^{V600E}$ splice variants. Both events increase $BRAF^{V600E}$ dimerization, rendering RAF inhibitors inefficient. Unlike melanoma, colorectal cancers (CRCs) express high amounts of EGFR, which is feedback suppressed by the high ERK activity caused by $BRAF^{V600E}$. Inhibiting $BRAF^{V600E}$ releases this negative feedback and allows the EGFR to activate RAS, which induces RAF dimerization and paradoxical pathway activation (Prahallad et al., 2012). Combining RAF with MEK inhibitors improved the response rate in $BRAF^{V600E}$-mutated CRC (Corcoran et al., 2015). Further adding an EGFR inhibitor generated high response rates and promising clinical results (Kopetz et al., 2019; Van Cutsem et al., 2019). Heterogeneity of RTK expression in genetically identical cells can also result in resistance to RAF inhibitors (Gerosa et al., 2020).

Using RAF as an example, we show that negative and positive feedback loops cannot lead to a complete, steady-state revival of the pathway output activity unless the inhibitor can induce RAF dimerization (Figures 5B and 5C). Paradox-breaking RAF inhibitors are thought to avoid paradoxical pathway activation by not inducing RAF dimerization (Karoulia et al., 2016). However, recent experiments showed that the paradox-breaking RAF inhibitor PLX8394 still induces paradoxical activation of ERK when cells overexpress

Author Manuscript Author Manuscript Author Manuscript Author Manuscript

14-3-3 proteins, which promote RAF dimerization (Mendiratta et al., 2019). Our model recapitulates these data. The overexpression of 14-3-3 not only counteracts the ability of a paradox-breaking RAF inhibitor to reduce ERK activity but it also even restores paradoxical ERK activation (Figure S8).

Our model, validation experiments, and previously reported data (Rukhlenko et al., 2018) suggest that a type I½ RAF inhibitor given together with a type II RAF inhibitor is an efficacious synergistic combination that counterbalances ERK pathway reactivation and concomitant drug resistance in NRAS mutant melanoma and AML cells. This two-RAF inhibitor treatment can be more effective than treatment with MEK and RAF inhibitors (Figures 6C–6E and S7). However, depending on the cell context and heterogeneity of tumor cells, the search for optimal drug combinations in different tumor types will require further dedicated research efforts.

In summary, our analysis has elaborated dynamic principles and network topologies that control drug responses of signaling pathways and revealed the mechanisms and extent of pathway reactivation if resistance occurs. These findings will be useful in informing the systematic improvement of combining existing drugs and feed into the discovery and development of smart future drugs that consider network context.

STAR★METHODS

RESOURCE AVAILABILITY

Lead contact—Further information and requests for resources and reagents should be directed to and will be fulfilled by the lead contact, Prof. Boris N. Kholodenko (boris.kholodenko@ucd.ie).

Materials availability—This study did not generate new unique reagents.

Data and code availability—The published article includes all datasets and codes generated or analyzed during this study.

EXPERIMENTAL MODEL AND SUBJECT DETAILS

Cell culture—MEL-JUSO cell line was purchased from DSMZ. OCI-AML-3 cell line was a gift from Prof. Ken Mills, Queen’s University Belfast. All cells were grown in RPMI 1640 supplemented with 2 mM L-glutamine and 10% (v/v) fetal bovine serum (all from GIBCO) in a humidified atmosphere of 5% CO_2 at 37°C.

For treatments, MEL-JUSO were seeded in 6-well plates (Greiner CELLSTAR dishes) at the density of 3×10^5 cells per well. OCI-AML-3 were seeded in 12-well plates at the density of 5×10^5/mL.

After reaching sufficient confluency respectively cell number, cells were treated with different concentrations of inhibitors and DMSO as control as indicated.

Author Manuscript Author Manuscript Author Manuscript Author Manuscript

METHOD DETAILS

RAF inhibitors—All inhibitors used in this study were purchased from Selleckchem Ltd: TAK-632 (#S7291), Trametinib (GSK1120212, #S2673), Cobimetinib (GDC-0973, #S8041), Vemurafenib (PLX4032, #1267), and Encorafenib (LGX818, #S7108).

Inhibitors were dissolved in DMSO and stocks were stored at −80°C.

Western blot—Total lysates for western blotting were prepared on ice using 10mM Tris-HCl pH 7.5, 150 mM NaCl, 0.5% (v/v) NP-40 (Calbiochem), complemented with COMPLETE Mini protease and PhosSTOP phosphatase inhibitor cocktails (both from Roche).

Cellular debris were removed from the lysate by centrifugation at 10,000 g at 4°C for 10 min. Following protein quantification using the Pierce BCA Protein Assay Kit (Thermo Scientific), lysates were adjusted to equal protein concentrations

Using the Mini Protean Tetra system (Bio-Rad), lysates were then resolved by SDS-PAGE (10% PAA) and transferred on a polyvinylidene difluoride membrane (Millipore).

Protein visualization was performed by the iBright CL750 Imaging System (Invitrogen), using horseradish peroxidase–conjugated secondary antibodies (Cell Signaling Technologies) and the enhanced chemiluminescence system (GE Healthcare) for the following antibodies: Polyclonal rabbit anti-human mitogen-activated protein (MAP) kinase (extra-cellular signal-regulated kinase (ERK) 1 & 2) antibody (Sigma #M5670), monoclonal mouse anti-human MAP kinase, activated (diphosphorylated ERK-1 & 2) antibody (Sigma #8159).

MSD multi-spot assay ELISA system—ERK activation was assessed by ELISA using the MESOSCALE MSD kit according to the manufacturer's instructions. Briefly, following the addition of complete MSD lysis buffer and scraping the cells from the surface of the dish, the cellular debris was removed from the lysate by centrifugation at 10000 g at 4°C for 10 min. Protein concentration was determined using the BCA test according to the manufacturer's instructions (Pierce BCA Protein Assay Kit). Lysates were adjusted to 0.1 μg/μL protein concentration and relative ERK activation was assessed according to the manufacturer's instructions using the MSD Sector Imager 2400 (model 1250).

Modeling

Systems-level responses to a drug: We consider a network comprising n independent state variables (x_i) assigned to each of n network nodes. Each variable x_i represents the concentration or activity level of a node i. The linearly dependent variables, such as inactive forms of proteins are expressed in terms of linearly independent variables x_i and moiety conservations. The dynamics of the system is given by mass balance equations,

$$\frac{d\boldsymbol{x}}{dt} = \boldsymbol{f}(\boldsymbol{x}, \boldsymbol{p}, I)\,.\ \ \boldsymbol{x} = x_1, \ldots, x_n, \boldsymbol{p} = p_1, \ldots, p_m\,. \qquad \text{(Equation 1.1)}$$

Author Manuscript Author Manuscript Author Manuscript Author Manuscript

Here $\boldsymbol{x}$ is the vector of independent variables (activities of network nodes), $\boldsymbol{p}$ is the parameter vector, I is the drug concentration, which for convenience is separated from the other parameters, such as reaction constants and the conserved moieties. $\boldsymbol{f}(\boldsymbol{x}, \boldsymbol{p}, I)$ is a function of these independent variables, parameters and drug concentration. The function $\boldsymbol{f}(\boldsymbol{x}, \boldsymbol{p}, I)$ is derived using the network stoichiometric matrix and the reaction rates (see, e.g., Bruggeman et al., 2002).

The Jacobian of this ordinary differential equation (ODE) system is the s by s matrix ($\boldsymbol{J}$) of the partial derivatives of the function $\boldsymbol{f}(\boldsymbol{x}, \boldsymbol{p}, I)$ with respect to the state variables $\boldsymbol{x}$,

$$\boldsymbol{J} = \frac{\partial \boldsymbol{f}(\boldsymbol{x}, \boldsymbol{p}, I)}{\partial \boldsymbol{x}}. \quad \text{(Equation 1.2)}$$

Given that the system has a single stable steady state, all eigenvalues of $\boldsymbol{J}$ are non-zero. The stationary activities of network nodes are found from the system of algebraic equations,

$$\boldsymbol{f}(\boldsymbol{x}, \boldsymbol{p}, I) = 0. \quad \text{(Equation 1.3)}$$

The matrix of the connectivity coefficients ($\boldsymbol{r}$) is defined as (Bastiaens et al., 2015; Kholodenko et al., 2002; Lill et al., 2019; Santra et al., 2018),

$$\boldsymbol{r} = -(dg\boldsymbol{J})^{-1} \cdot \boldsymbol{J} = -\left(\boldsymbol{dg}\left(\frac{\partial \boldsymbol{f}(\boldsymbol{x}, \boldsymbol{p}, I)}{\partial \boldsymbol{x}}\right)\right)^{-1} \cdot \frac{\partial \boldsymbol{f}(\boldsymbol{x}, \boldsymbol{p}, I)}{\partial \boldsymbol{x}}. \quad \text{(Equation 1.4)}$$

Here $dg\boldsymbol{F}\cdot$ is the diagonal matrix that contains the diagonal elements of the matrix $\boldsymbol{F}$.

The local response of a node x_i to a drug is defined by a partial derivative $\partial x_i/\partial I$, assuming that all other nodes are kept fixed, that is

$$\frac{\partial x_i(\boldsymbol{p}, I)}{\partial I} = -\frac{\partial f_i(x_1, \ldots, x_n, \boldsymbol{p}, I)/\partial I}{\partial f_i(x_1, \ldots, X_n, \boldsymbol{p}, I)/\partial x_i}\Bigg|_{steady\ state\ of\ module\ i}. \quad \text{(Equation 1.5)}$$

The vector of local responses ($\boldsymbol{r}_{xI}$) of network nodes to a drug is expressed as in Kholodenko et al. (2002),

$$\boldsymbol{r}_{xI} = \frac{\partial \boldsymbol{x}}{\partial I} = -\left(\boldsymbol{dg}\left(\frac{\partial \boldsymbol{f}(\boldsymbol{x}, \boldsymbol{p}, I)}{\partial \boldsymbol{x}}\right)\right)^{-1} \cdot \frac{\partial \boldsymbol{f}(\boldsymbol{x}, \boldsymbol{p}, I)}{\partial I} = = -(dg\boldsymbol{J})^{-1} \cdot \frac{\partial \boldsymbol{f}(\boldsymbol{x}, \boldsymbol{p}, I)}{\partial I}. \quad \text{(Equation 1.6)}$$

The vector of the global, systems-level responses of network nodes to a drug is defined as,

$$\boldsymbol{R}_{xI} = \frac{dx}{d\mathrm{I}}\Bigg|_{\text{system steady state}} \quad \text{(Equation 1.7)}$$

Differentiating Equation 1.3, we obtain,

$$\frac{\partial \boldsymbol{f}(\boldsymbol{x}, \boldsymbol{p}, I)}{\partial \boldsymbol{x}} \cdot \boldsymbol{R}_{xI} = \boldsymbol{J} \cdot \boldsymbol{R}_{xI} = -\frac{\partial \boldsymbol{f}(\boldsymbol{x}, \boldsymbol{p}, I)}{\partial I} \quad \text{(Equation 1.8)}$$

Author Manuscript Author Manuscript Author Manuscript Author Manuscript

Multiplying both sides by the inverse of the Jacobin matrix and using Equations 1.4, 1.5, and 1.6, we finally obtain,

$$\boldsymbol{R_{xI}} = -\left(\frac{\partial \boldsymbol{f}(\boldsymbol{x},\boldsymbol{p},I)}{\partial \boldsymbol{x}}\right)^{-1}\cdot\frac{\partial \boldsymbol{f}(\boldsymbol{x},\boldsymbol{p},I)}{\partial I} = -(\boldsymbol{r})^{-1}\cdot\boldsymbol{r}_{xI}\,. \qquad \text{(Equation 1.9)}$$

Equation 1.9 provides a general expression of the systems-levels responses to a drug in the matrix format.

The global, systems-level responses and local responses, which are components of the connectivity matrix $\boldsymbol{r}$ or the vector $\boldsymbol{r}_{xI}$ of the local responses of the primary targets to the drug, can also be expressed in dimensional units, using log-to-log derivatives (Kholodenko et al., 2002). Next, we show that Equation 1.9 also holds for logarithmic derivatives.

The matrix of the connectivity coefficients defined using log-to-log derivatives, $\boldsymbol{r_{log}}$ = (∂ln x_i/∂ln x_j), is given by,

$$\boldsymbol{r}_{log} = \frac{\partial \ln x_i}{\partial \ln x_j} = \begin{pmatrix} -1 & \frac{\partial x_1}{\partial x_2}\cdot\frac{x_2}{x_1} & \cdots & \frac{\partial x_1}{\partial x_n}\cdot\frac{x_n}{x_1} \\ \frac{\partial x_2}{\partial x_1}\cdot\frac{x_1}{x_2} & -1 & \cdots & \frac{\partial x_2}{\partial x_n}\cdot\frac{x_n}{x_2} \\ \vdots & \vdots & \ddots & \vdots \\ \frac{\partial x_n}{\partial x_1}\cdot\frac{x_1}{x_n} & \frac{\partial x_n}{\partial x_2}\cdot\frac{x_2}{x_n} & \cdots & -1 \end{pmatrix} = \begin{pmatrix} \frac{1}{x_1} & 0 & \cdots & 0 \\ 0 & \frac{1}{x_2} & \cdots & 0 \\ \vdots & \vdots & \ddots & \vdots \\ 0 & 0 & \cdots & \frac{1}{x_n} \end{pmatrix}\cdot\begin{pmatrix} -1 & \frac{\partial x_1}{\partial x_2} & \cdots & \frac{\partial x_1}{\partial x_n} \\ \frac{\partial x_2}{\partial x_1} & -1 & \cdots & \frac{\partial x_2}{\partial x_n} \\ \vdots & \vdots & \ddots & \vdots \\ \frac{\partial x_n}{\partial x_1} & \frac{\partial x_n}{\partial x_2} & \cdots & -1 \end{pmatrix}\cdot\begin{pmatrix} x_1 & 0 & \cdots & 0 \\ 0 & x_2 & \cdots & 0 \\ \vdots & \vdots & \ddots & \vdots \\ 0 & 0 & \cdots & x_n \end{pmatrix}$$
$$= (diag\,x)^{-1}\cdot\boldsymbol{r}\cdot(diag\,x)$$

The vector of global responses (R_{xI}^{log}) defined using log-to-log derivatives is expressed as follows,

$$\boldsymbol{R}_{xI}^{log} = \frac{d\ln\boldsymbol{x}}{d\ln I}\Big|_{\text{system steady state}} = (diag\,x)^{-1}\cdot\boldsymbol{R}_{xI}\cdot I$$

The vector of local responses ($\boldsymbol{r}_{xI}^{log}$) of network nodes to a drug (I) defined using log-to-log derivatives is given by,

$$\boldsymbol{r}_{xI}^{log} = \frac{\partial\ln\boldsymbol{x}}{\partial\ln I} = (diag\,x)^{-1}\cdot\boldsymbol{r}_{xI}\cdot I$$

Equation 1.9 can be re-written as

$$\boldsymbol{r}\cdot\boldsymbol{R}_{xI} = -\boldsymbol{r}_{xI}$$

Multiplying both sides of this equation by ($diag\,x$) $^{-1}\cdot I$, we obtain,

Author Manuscript Author Manuscript Author Manuscript Author Manuscript

$$(diag\,x)^{-1}\cdot \boldsymbol{r}\cdot (diag\,x)(diag\,x)^{-1}\boldsymbol{R}_{xI}\cdot I = -(diag\,x)^{-1}\cdot \boldsymbol{r}_{xI}\cdot I$$
$$\boldsymbol{r}_{log}\cdot \boldsymbol{R}_{xI}^{log} = -\boldsymbol{r}_{xI}^{log} \qquad \text{(Equation 1.10)}$$
$$\boldsymbol{R}_{xI}^{log} = -\left(\boldsymbol{r}_{log}\right)^{-1}\cdot \boldsymbol{r}_{xI}^{log}.$$

Equations 1.9 and 1.10 show that the same expression is valid for both usual derivatives and logarithmic derivatives.

The expression for the global, systems-level responses to the drug, Equation 1.9, involves the inverse of the connection coefficient matrix, which in turn is expressed as the inverse of the normalized Jacobian matrix, which depends on the stoichiometry matrix and rate expressions (Bruggeman et al., 2002). Nevertheless, it is instructive to derive several simple equations that are given in the main text directly, rather than using software tools for matrix inversions that require exactly defining the number of nodes and the matrix size. These derivations are intuitively transparent and emphasize key topological features of pathways with any primary drug targets and arbitrary number of constituents. We present these derivations below.

Drug response of a pathway with a single feedback loop: Following a change in the drug dose (ΔI), the system-wide (or global) change in the activity (ΔX_1) of the kinase at the first level is expressed in terms of the global change in the activity (ΔT) of the target and ΔI and the connection coefficients, r_{X_1T} and r_{X_1I}, as follows,

$$\Delta X_1 = r_{X_1T}\cdot \Delta T + r_{X_1I}\cdot \Delta I\,. \qquad \text{(Equation 2.1)}$$

The changes in the X_j activity at level j occur only due to the changes in the activity of X_{j-1}. The changes in T occur only through changes in X_{N-1}, see Figure 2A,

$$\Delta T = r_{TX_{N-1}}\cdot r_{X_{N-1}X_{N-2}}\cdot \ldots \cdot r_{X_2X_1}\cdot \Delta X_1 = P\cdot \Delta X_1\,. \qquad \text{(Equation 2.2)}$$

Substituting Equation 2.1 in Equation 2.2, and proceeding to the limit of infinitesimal changes, we arrive at Equation 5 of the main text.

Mechanistic models of a 3-tier signaling cascade with negative feedback: Mass-action models schematically depicted in Figures 2B, 2F, and S1B describe elementary enzymatic steps of every reaction catalyzed by each kinase and phosphatase in a 3-tier signaling cascade. The pathway shown in Figure 2B resembles a three-tier MAPK pathway where kinases X_2 and T are phosphorylated on two sites for full activation. In the pathways shown in Figures 2F and S1B kinases X_2 and T have only two forms, one is inactive and the other isactive. Negative feedback from the output protein to the first tier kinase X_1 is mediated either by the inhibitory phosphorylation of X_1 by T (Figures 2B and S1B) or by the formation of an inactive complex between X_1 and T, sequestering the active kinase (Figure 2F). The primary target of an inhibitor (I) is the first-tier kinase (Figures 2B and 2F) or a kinase within a negative feedback loop (Figure S1B). In the models depicted in Figures 2B and S1B, the inhibitor I can bind to inactive (X_1^i), active (X_1) and feedback-modified (X_1^P)

Author Manuscript Author Manuscript Author Manuscript Author Manuscript

forms of the first-tier kinase, and to inactive (X_2^i) and active (X_2) forms, respectively. In the model shown in Figure 2F, the inhibitor I binds to inactive (X_1^i) and active (X_1) forms of the first-tier kinase, which is also sequestered by T.

Phosphorylation or PTM-mediated feedback: Multiple forms of the kinase X_1 (active, inactive, modified by feedback from T, free or bound to an inhibitor) generate a large number of the corresponding mass-action reactions. A rule-based approach overcomes the necessity of manual enumeration of state variables, using formalizations called 'rules', which account for combinatorial processes that may proceed simultaneously (Borisov et al., 2008; Chylek et al., 2014; Varga et al., 2017). Our mass-action, mechanistic model is written using the BNGL format and BioNetGen software (Chylek et al., 2014). Mass action reaction laws, equations and the rate and dissociation constants are given in the SBML format in Data S1.

Protein sequestration mediated feedback: the output protein T and the upstream kinase $\boldsymbol{X}_1$ form an inactive complex [$\boldsymbol{X}_1$-T]: Consider the kinetic scheme depicted in Figure 2F. Following binding of a drug (I) to its primary target X_1 the moiety conservations for X_1 and T read,

$$X_1^i + X_1 + [X_1 - T] + [X_1 - I] = X_1^{tot}\,. \qquad \text{(Equation 3.1)}$$

$$[X_1 - T] + T + T^i = T^{tot}\,. \qquad \text{(Equation 3.2)}$$

From Equations 3.1 and 3.2 concentration of (X_1^i) and can T^i be expressed as functions of X_1, T and I,

$$\begin{aligned} X_1^i &= f_1(X_1, T, I) \\ T^i &= f_2(X_1, T, I)\,. \end{aligned} \qquad \text{(Equation 3.3)}$$

Therefore, even when all other pathway components are kept constant, both X_1 and T locally respond to the changing drug dose. The changes in the concentrations of these two species after a change in the drug dose are related by the following equation,

$$\begin{aligned} &\Delta X_1^i + \Delta X_1 + (T/K_T)\Delta X_1 + (X_1/K_T)\Delta T + (I/K_I)\Delta X_1 + (X_1/K_I)\Delta I \\ &= 0. \end{aligned} \qquad \text{(Equation 3.4)}$$

Here K_T and K_I are dissociation constants of the complexes [X_1-T] and [X_1-I], respectively. The change (dX_1^i) in the concentration of (X_1^i) is expressed as,

$$\Delta X_1^i = (\partial f_1/\partial X_1)dX_1 + (\partial f_1/\partial T)dT + (\partial f_1/\partial I)dI\,. \qquad \text{(Equation 3.5)}$$

From Equation 3.2 we obtain,

Author Manuscript Author Manuscript Author Manuscript Author Manuscript

$$(T/K_T)\Delta X_1 + (X_1/K_T)\Delta T + \Delta T + \Delta T^i = 0$$
$$\Delta T^i = (\partial f_2/\partial T)\Delta T + (\partial f_2/\partial X_1)\Delta X_1 + (\partial f_2/\partial I)\Delta I\,. \quad \text{(Equation 3.6)}$$

Equations 3.4, 3.5, and 3.6 allow expressing ΔX_1 and ΔT in terms of dI and the local response coefficients $r_{X_1 I} = \partial X_1/\partial I$ and $r_{TI} = \partial T/\partial I$,

$$\Delta X_1 = r_{X_1 T}\Delta I + r_{X_1 T}\Delta T\,. \quad \text{(Equation 3.7)}$$

$$\Delta T = \left(r_{X_2 X_1}\cdot \ldots \cdot r_{T X_N}\right)\Delta X_1 + r_{TI}\Delta I = P\cdot \Delta X_1 + r_{TI}\Delta I\,. \quad \text{(Equation 3.8)}$$

Substituting Equation 3.7 into Equation 3.8 we obtain the expression of the systems-level response, $R_{X_1 I} = \Delta X_1/\Delta I$, in terms of the local responses,

$$R_{X_1 I} = \frac{r_{X_1 I} + r_{X_1 T} r_{TI}}{1 - r_{X_1 T} P}\,. \quad \text{(Equation 3.9)}$$

Obviously, $r_{X_1 I} < 0$ and $r_{X_1 T} < 0$. As T and I compete for binding to X_1, free T increases as I increases and $r_{TI} > 0$. Then, the systems-level response to the drug will always be negative, $R_{X_1 I} < 0$, ruling out paradoxical activation responses to the inhibitor. Figure 2G illustrates this conclusion for a mechanistic mass-action model schematically depicted in Figure 2F. Data S2 gives mass action reaction laws, equations, and the rate and dissociation constants for this model in SBML format.

Systems-level responses to the inhibition of an intermediate kinase: A pathway of phosphorylation-dephosphorylation cycles arranged as sequential cascade combined with a negative feedback resembles a so-called ‘negative feedback amplifier’ where the negative feedback reduces the effects of input noise and buffers changes within the amplifier (Sturm et al., 2010). Here we analyze the systems responses to a drug that affects an intermediate kinase (X_m), $1 < m < N$, located within a negative feedback loop from the output T to the upstream kinase X_1 (Figure S1A). The changes in the activities of cascade kinases (ΔX_i) following the change in the drug dose (ΔI) are expressed as follows,

$$\begin{aligned}
&\Delta X_1 = r_{X_1 T}\cdot \Delta T\\
&\Delta X_2 = r_{X_2 X_1}\cdot \Delta X_1\\
&\Delta X_{m-1} = r_{X_m x_{m-1}}\cdot \ldots \cdot r_{X_2 X_1}\cdot \Delta X_1\\
&\Delta X_m = r_{X_m X_{m-1}}\cdot \ldots \cdot r_{X_2 X_1}\cdot \Delta X_1 + r_{X_m I}\cdot \Delta I = P_1\cdot \Delta X_1 + r_{X_m I}\cdot \Delta I\\
&\Delta T = r_{T X_{N-1}}\cdot r_{X_{N-1} X_{N-2}}\cdot \ldots \cdot r_{X_{m+1} X_m}\cdot \Delta X_m = P_m\cdot \Delta X_m\,.
\end{aligned} \quad \text{(Equation 4.1)}$$

Rearranging, we obtain,

$$\Delta T = P_m\cdot P_1\cdot \Delta X_1 + P_m\cdot r_{X_m I}\cdot \Delta I = P\cdot r_{X_1 T}\cdot \Delta T + P_m\cdot r_{X_m I}\cdot \Delta I\,. \quad \text{(Equation 4.2)}$$

In the limit of infinitesimal changes we obtain,

Author Manuscript Author Manuscript Author Manuscript Author Manuscript

$$R_{TI} = \frac{r_{X_m I} \cdot P_m}{1 - r_{X_1 T} \cdot P}; P_m = r_{X_{m+1} X_m} \cdot \ldots \cdot r_{T X_{N-1}} < P. \quad \text{(Equation 4.3)}$$

In particular, if the drug affects the output kinase, then the systems response of the output T to the drug I is the following,

$$R_{TI} = \frac{r_{TI}}{1 - r_{X_1 T} \cdot P}. \quad \text{(Equation 4.4)}$$

Drug response of a pathway featuring intertwined negative and positive feedback loops: Given the network architecture shown in Figure 2H, the systems-wide changes in the activities of the kinase X_1, the pathway target T and the kinases Y and Z (that mediate positive and negative influence of T on X_1) can be related to the change in the drug dose (I) as follows,

$$\begin{aligned} \Delta X_1 &= r_{X_1 Y} \cdot \Delta Y + r_{X_1 Z} \cdot \Delta Z + r_{X_1 I} \cdot \Delta I \\ \Delta Y &= r_{YT} \cdot \Delta T;\ \Delta Z = r_{ZT} \cdot \Delta T \\ \Delta T &= r_{T X_{N-1}} \cdot r_{X_{N-1} X_{N-2}} \cdot \ldots \cdot r_{X_2 X_1} \cdot \Delta X_1 = P \cdot \Delta X_1. \end{aligned} \quad \text{(Equation 5.1)}$$

Equation 6 of the main text can be readily obtained from Equation 5.1.

Transient pathway reactivation by expression of negative feedback regulators: The dynamics of the pathway shown in Figure 3A are governed by the following equations,

$$\begin{aligned} \frac{d[MKK]}{dt} &= \frac{V_{MKKa} S\left(MKK^{tot} - MKK\right)}{K_{MKKa} + \left(MKK^{tot} - MKK\right)} \cdot \frac{1 + \gamma_{JNK}[JNK]/K_\gamma}{1 + [JNK]/K_\gamma} - \frac{V_{MKK}[MKK]}{K_{MKK} + MKK} \\ \frac{d[JNK]}{dt} &= \frac{V_{JNKa}[JNK]\left(JNK^{tot} - [JNK]\right)}{K_{JNKa} + \left(JNK^{tot} - [JNK]\right)} \cdot \frac{1}{1 + I_{JNK}/K_d^{IJNK}} - \frac{\left(V_{JNK} + V_{JNK}^{DUSP}[DUSP]\right)[JNK]}{K_{JNK} + [JNK]} \\ \frac{d[dusp]}{dt} &= \frac{V_{duspa}[JNK]^2}{K_{duspa}^2 + [JNK]^2} - V_{dusp}[dusp] \\ \frac{d[DUSP]}{dt} &= V_{DUSPa}[dusp] - V_{DUSP}[DUSP] \end{aligned} \quad \text{(Equation 6.1)}$$

.

Parameters are given in Table S1.

The time course presented in Figure 3B was calculated using Equation 6.1 and parameters in Table S1.

The integral feedback: Approximate description of the transient control by negative feedback regulators: Consider expression of a negative feedback regulator (*NR*) induced by a MAPK kinase (*MAPK*). This negative regulator can inhibit upstream signaling by dephosphorylation, e.g., a phosphatase (DUSP), or bind to and inhibit other upstream proteins, e.g., receptor tyrosine kinases *RTK*. Assuming that the negative regulator decays slower than the inhibition time, an approximate dynamic description reads as follows (Goyal et al., 2017; Nakakuki et al., 2010),

Author Manuscript Author Manuscript Author Manuscript Author Manuscript

$$\frac{d[RTK]}{dt} = k_a\left[RTK^i\right] - k_i[RTK] - k_{NR}[RTK][NR]$$
$$\frac{d[MAPK]}{dt} = k_a\left[MAPK^i\right] \cdot [RTK] - k_i[MAPK] \quad \text{(Equation 7.1)}$$
$$\frac{d[NR]}{dt} = k_{sNR}[MAPK]\,.$$

From Equation 7.1 it follows that,

$$[NR] = k_{sNR}\int [MAPK]dt\,. \quad \text{(Equation 7.2)}$$

After substitution of Equation 7.2 into Equation 7.1 we obtain a system of equations with integral negative feedback. However, Equation 7.2 shows that the concentration of *NR* never reaches a steady state, increasing infinitely with time. At the same time, a non-zero degradation rate of *NR* breaks down integral feedback in this system.

Perfect adaption to a drug cannot be reached using integral feedback in generic signaling networks with moiety conservations: Here we demonstrate that a complete reactivation of signaling outputs after drug inhibition is not achieved by so-called antithetic integral feedback (Aoki et al., 2019; Briat et al., 2016) in a generic cell signaling networks where the moieties of interconverted, active and inactive, protein forms are conserved. The existence of moiety conservations of interconverted protein forms is a rule rather than an exception in kinase signaling networks. These moiety conserved cycles violate an assumption of a key theorem, which proves complete or perfect adaptation of the systems output to a fixed set-point, i.e., the desired output value, owing to antithetic integral feedback. Theorem 2 in Briat et al. (2016) assumes the accessibility of the desired asymptotic set-point state. In other words, a unique systems steady state with the desired output level should be accessible, following a perturbation. Below we show that in biochemical systems with moiety conserved cycles, there are multiple primary drug targets, whose perturbations make the desired steady state inaccessible because of the upper limit to the abundance of either the target or downstream proteins that transfer the signal. In mathematical terms, the moiety conservations bring about saturation nonlinearity of a network transfer function (Na et al., 2018).

Generic signaling networks that contain antithetic integral feedbacks are depicted in Figures S2A and S2B. These networks satisfy the antithetic integral feedback requirements formulated in Briat et al. (2016). A generic network shown in Figure S2A has arbitrary signaling constituents and connections between them, but the total abundance of interconvertible forms of the upstream primary drug target X_1, which is regulated by the antithetic integral feedback control module consisting of species Y_1 and Y_2, is conserved (X_1^{tot}). In a generic network depicted in Figure S2B, the abundance of the feedback-regulated signaling protein X_1 is not conserved, as it can degrade and be rapidly synthesized *de novo*. However, in the network module, which has arbitrary signaling topology and transfers the signal via the module output (X_S) downstream to the primary drug target (X_D) and the

Author Manuscript Author Manuscript Author Manuscript Author Manuscript

signaling output (T), intercomvertible protein forms for at least one or more proteins are constrained by moiety conservations.

The presence of the antithetic feedback module shown in Figures S2A and S2B has been proven to be a necessary condition and not only a sufficient condition of robust perfect adaptation in chemical networks (Aoki et al., 2019). The dynamics of the species, Y_1 and Y_2, in the integral control module are described by the following equations,

$$\begin{aligned} \frac{dY_1}{dt} &= \mu - \eta \cdot Y_1 \cdot Y_2 \\ \frac{dY_2}{dt} &= \theta \cdot T - \eta \cdot Y_1 \cdot Y_2 . \end{aligned} \qquad \text{(Equation 7.3)}$$

Here μ is the constant rate of synthesis of Y_1, θ is the rate constant of T-induced synthesis of Y_2, η is the rate constant of annihilation reaction of Y_1 and Y_2 (degradation of the $Y_1 Y_2$ complex).

Subtracting the equation for dY_2/dt from the equation for dY_1/dt yields,

$$\frac{d(Y_1 - Y_2)}{dt} = \mu - \theta \cdot T . \qquad \text{(Equation 7.4)}$$

Then, the difference between Y_1 and Y_2 concentrations is expressed as,

$$Y_1 - Y_2 = \int (\mu - \theta \cdot T) dt . \qquad \text{(Equation 7.5)}$$

This expression represents integral feedback and shows that there can only be a single steady state where $T = \mu/\theta$. However, this set-point steady state cannot be reached following a multitude of different perturbations.

Consider a perturbation to the network presented in Figure S2A by a drug that binds the upstream primary target. Since its total abundance is conserved (X_1^{tot}), the maximal concentration of an active form (X_1) is limited by X_1^{tot} value, i.e., $X_1 \leq X_1^{tot}$. Then, if an inhibitor (I) of X_1 is added, the maximal concentration of inhibitor-free X_1 satisfies the following inequality,

$$X_1 \leq X_1^{tot} \cdot \frac{1}{1 + \frac{I}{K_d}}$$

Here I and K_d are the inhibitor concentration and dissociation constant, respectively. In this case, for every value of set-point μ/θ there exists a value of inhibitor concentration I, which can make the X_1 activity to be arbitrarily small. Since the steady state concentration of the network output T is a function (F) of X_1, i.e., $T = F(X_1)$, then for every value of set-point μ/θ there exists inhibitor concentration that will make the T activity close to $F(0) \neq \mu/\theta$. This proves that if the total abundance of primary drug target is conserved, the steady-state set-

Author Manuscript Author Manuscript Author Manuscript Author Manuscript

point cannot be reached and the perfect reactivation of signaling output cannot be reached for an arbitrary network.

For the network shown in Figure S2B, consider a perturbation by an inhibitor that binds the downstream primary target X_D. Owing moiety conservations there is saturation nonlinearity of transfer function of the network module that transfers the signal from X_1 to X_D via the module output (X_S). Let X_S^{max} be the maximal value of the output of this module. Since the primary drug target, X_D, is activated by X_S, its activity is a monotonous function (G) of X_S,

$$X_D = G(X_S)$$

Then, the maximal value of X_D is $G(X_S^{max})$. When the primary target is inhibited by I, the value of X_D cannot exceed the following,

$$X_D \leq G\left(X_S^{max}\right) \cdot \frac{1}{1 + \frac{1}{K_d}}$$

Therefore, for each value of set-point μ/θ there exists a value of inhibitor concentration I, which can make concentration of X_D to be arbitrarily small. Since T is activated by X_D, this makes the T activity to be near the activity that corresponds to $X_D = 0$, which rules out reaching the set-point value μ/θ and fully reactivating the network output.

We conclude that if (*i*) the regulated network contains the modules with saturation nonlinearity of transfer function, and (*ii*) these modules cannot be bypassed, and (*iii*) there are no modules with transfer function singularity, then the accessibility condition can be violated by drug perturbations downstream of any module with transfer function saturation nonlinearity. In control engineering the proof of this statement is known and based on the properties of multiplication of transfer functions for sequentially connected modules along the path (Bakshi and Goyal, 2007).

Antithetic integral feedback motif in networks with moiety conservations—examples: Consider a signaling pathway, which is controlled by two species (Y_1 and Y_2) and has the required key properties of the antithetic integral feedback controller (Figure 3C). In this pathway, the rate of conversion of an inactive form X_1^i of the upstream kinase X_1 into its active form is stimulated by the controlling protein Y_1. X_1 activates the output T through a cascade of intermediate kinases, X_2, …, X_{n-1}. The first controlling protein Y_1 is synthesized in an external process, which has a constant rate and does not depend on signaling output or other pathway species. The output T of the regulated pathway induces expression of the second controlling protein Y_2 that forms a complex with Y_1, which subsequently degrades. The kinetic behavior of this network are governed by Equation 7.6,

Author Manuscript Author Manuscript Author Manuscript Author Manuscript

$$\begin{aligned}
\frac{dX_1}{dt} &= \frac{V_{X1a}S\left(X_1^{tot}-X_1\right)}{K_{X1a}+\left(X_1^{tot}-X_1\right)}\cdot\frac{1+\gamma Y_1/K_d^{\gamma}}{1+Y_1/K_d^{\gamma}}\cdot\frac{1}{1+I_{X1}/K_d^{IX1}}-\frac{V_{X1}X_1}{K_{X_1}+X_1}\\
\frac{dX_2}{dt} &= \frac{V_{X2a}X_1\left(X_2^{tot}-X_2\right)}{K_{X2a}+\left(X_2^{tot}-X_2\right)}\cdot\frac{1}{1+I_{X2}/K_d^{IX2}}-\frac{V_{X2}X_2}{K_{x2}+X_2}\\
\frac{dT}{dt} &= \frac{V_{Ta}X_2\left(T^{tot}-T\right)}{K_{Ta}+\left(T^{tot}-T\right)}\cdot\frac{1}{1+I_T/K_d^{IT}}-\frac{V_TT}{K_T+T}\\
\frac{dY_1}{dt} &= \mu\cdot\frac{1}{1+I_{Y1}/K_d^{IY1}}-\eta Y_1Y_2\\
\frac{dY_2}{dt} &= \theta T-\eta Y_1Y_2\,.
\end{aligned}\qquad \text{(Equation 7.6)}$$

Here in Equation 7.6 and below in Equations 7.7 and 7.8, V_{X1a}, V_{X2a} and V_{Ta}, and K_{X1a}, K_{X2a} and K_{Ta} are the maximal rates and Michaelis constants of activation of X_1, X_2 and T, respectively, and V_{X1}, V_{X2} and V_T, and K_{X1}, K_{X2} and K_T are the maximal rates and Michaelis constants of deactivation of X_1, X_2 and T, respectively. S is the level of input activation. μ is the constant rate of synthesis of Y_1, θ is the rate constant of T-induced synthesis of Y_2, η is the rate constant of annihilation reaction of Y_1 and Y_2 (degradation of the Y_1Y complex). I_{X1}, I_{X2}, I_T and I_{Y1}, and K_d^{IX1}, K_d^{IX2}, K_d^{IT} and K_d^{IY1} are the concentrations and dissociation constants of inhibitors of X_1, X_2, T and Y_1, respectively.

Numerical solutions to Equation 7.6 demonstrate that although this network and its controller motif implements the integral feedback design (STAR Methods), there is no complete revival or overshoot of steady state output signaling after the inhibition of either the upstream kinase X_1, any intermediate kinases, X_2, …, X_{n-1}, or the output T by a drug I (Figures 3D and 3E). The presence of this antithetic integral controller motif was proven to be a necessary and sufficient condition for perfect adaptation in biomolecular networks (Aoki et al., 2019), but neither condition holds for networks that transfer signals via PTM cycles with conserved moieties of interconvertible proteins (Figures 3D and 3E).

In the second network example the controlling protein Y_1 directly catalyzes rather than facilitates the conversion of the inactive kinase form X_1^i into an active form X_1 (Figure S2C). The kinetic behavior of this network is determined by Equation 7.7,

$$\begin{aligned}
\frac{dX_1}{dt} &= \frac{V_{X1a}(S+Y_1)\left(X_1^{tot}-X_1\right)}{K_{X1a}+\left(X_1^{tot}-X_1\right)}\cdot\frac{1}{1+I_{X1}/K_d^{IX1}}-\frac{V_{X1}X_1}{K_{X1}+X_1}\\
\frac{dX_2}{dt} &= \frac{V_{X2a}X_1\left(X_2^{tot}-X_2\right)}{K_{X2a}+\left(X_2^{tot}-X_2\right)}\cdot\frac{1}{1+I_{X2}/K_d^{IX2}}-\frac{V_{X2}X_2}{K_{X2}+X_2}\\
\frac{dT}{dt} &= \frac{V_{Ta}X_2\left(T^{tot}-T\right)}{K_{Ta}+\left(T^{tot}-T\right)}\cdot\frac{1}{1+I_T/K_d^{IT}}-\frac{V_TT}{K_T+T}\\
\frac{dY_1}{dt} &= \mu\cdot\frac{1}{1+I_{Y1}/K_d^{IY1}}-\eta Y_1Y_2\\
\frac{dY_2}{dt} &= \theta T-\eta Y_1Y_2\,.
\end{aligned}\qquad \text{(Equation 7.7)}$$

Author Manuscript Author Manuscript Author Manuscript Author Manuscript

The difference between equations that describe these two networks above is that Y_1 is an activator of the catalytic conversion of an inactive form X_1^i into an active form X_1 in Equation 7.6. This is described by a hyperbolic multiplier (a common description of enzyme activation (Tsyganov et al., 2012)) where K_d^γ is an effective Michaelis constant, and $\gamma > 1$ is an activation coefficient. In Equation 7.7, Y_1 directly catalyzes rather than facilitates the conversion of an inactive kinase form into its active form. The solutions to Equation 7.7 clearly show that this signaling networks still lacks perfect signaling revival following drug inhibition of any kinase, X_1, X_2, …, X_{n-1}, the output T or the synthesis of the controlling protein Y_1 (Figures S2D and S2E).

In our third network example, the first controlling protein Y_1 induces the synthesis of the inactive upstream kinase (X_1^i) rather than catalyzing or facilitating its transition into an active form. The kinetic behavior of this network is described as follows,

$$\begin{aligned}
\frac{dX_1^i}{dt} &= V_{X1}^{syn} + V_{X1Y1}\cdot Y_1 + \frac{V_{X1}X_1}{K_{X1}+X_1} - V_{X1}^{deg}X_1 - \frac{V_{X1a}SX_1^i}{K_{X1a}+X_1^i}\cdot\frac{1}{1+I_{X1}/K_d^{IX1}}\\
\frac{\partial X_1}{\partial t} &= \frac{V_{X1a}SX_1^i}{K_{X1a}+X_1^i}\cdot\frac{1}{1+I_{X1}/K_d^{IX1}} - \frac{V_{X1}X_1}{K_{x1}+X_1}\\
\frac{dX_2}{dt} &= \frac{V_{X2a}X_1\left(X_2^{tot}-X_2\right)}{K_{X2a}+\left(X_2^{tot}-X_2\right)}\cdot\frac{1}{1+I_{X2}/K_d^{IX2}} - \frac{V_{x2}X_2}{K_{X2}+X_2}\\
\frac{dT}{dt} &= \frac{V_{Ta}X_2\left(T^{tot}-T\right)}{K_{Ta}+\left(T^{tot}-T\right)}\cdot\frac{1}{1+I_T/K_d^{IT}} - \frac{V_TT}{K_T+T}\\
\frac{dY_1}{dt} &= \mu\cdot\frac{1}{1+I_{Y1}/K_d^{IY1}} - \eta Y_1Y_2\\
\frac{dY_2}{dt} &= \theta T - \eta Y_1Y_2
\end{aligned}$$

(Equation 7.8)

.

Here the rate constants, $V_{X1\,Y1}\cdot V_{X1}^{syn}$ and V_{X1}^{deg}, are the basic rates of the X_1^i synthesis and degradation, respectively. Only this network design can show complete output reactivation, or perfect adaptation, in response to inhibiting the kinases X_1 or X_2 (Figures 3F–3H). However, inhibition of any other kinase, X_3, …, X_{n-1}, or the output T (Figure 3G, orange curve) necessarily leads to pathway inhibition. In addition, the inhibition of the controller Y_1 synthesis by a drug or the drug-induced direct degradation of the second controlling protein Y_2 rules out complete reactivation of output signaling (Figure 3G, green curve). Moreover, because signaling reactivation is brought about by the synthesis of an inactive kinase form, even when the reactivation is possible, it might take several days after drug treatment (Figure 3H).

The signaling networks shown in Figures 3C, 3F, and S2C have the controlling and regulated modules, implementing the topological properties that are reported to be necessary and sufficient for integral feedback (Aoki et al., 2019; Briat et al., 2016). Yet, these networks cannot perfectly adapt to drug inhibition of a number of targets. We conclude that the necessary and sufficient conditions to achieve the complete signaling recovery are not fulfilled for mammalian networks with the conserved abundances of interconverted protein forms.

Author Manuscript Author Manuscript Author Manuscript Author Manuscript

Parameters for Equations 7.6, 7.7, and 7.8 are given in Table S1.

For all three networks (Equations 7.6, 7.7, and 7.8), by subtracting the equation for dY_2/dt from the equation for dY_1/dt, we obtain,

$$\frac{d(Y_1 - Y_2)}{dt} = \mu \cdot \frac{1}{1 + I_{Y1}/K_d^{IY1}} - \theta T \,. \qquad \text{(Equation 7.9)}$$

Then, the difference between Y_1 and Y_2 concentrations is expressed as,

$$Y_1 - Y_2 = \int \left(\mu \cdot \frac{1}{1 + I_{Y1}/K_d^{IY1}} - \theta T \right) dt \,. \qquad \text{(Equation 7.10)}$$

This expression constitutes integral feedback and shows there can only be a single steady state where $T = (\mu/\theta)/\left(1 + I_{Y1}/K_d^{IY1}\right)$. Thus, at first glance any deviations of T from this steady state value will lead to re-adjustment of the concentrations of Y_1 and Y_2 until a steady state is reached. However, for the networks in Figures 3C and S2C, described by Equations 7.6 and 7.7, there is no perfect reactivation of the steady-state output signaling after the inhibition of either the upstream kinase X_1 or any of the intermediate kinases, X_2, …, X_{n-1} (Figures 3D and S2D, blue curves). The reason is that in these signaling networks (Equations 7.6 and 7.7) a conversion of an inactive kinase form (X_1^i) into an active form (X_1) has a limit determined by the moiety conservation of activation and inactivation forms, $X_1^i + X_1 = X_1^{tot}$, which is a feature of signaling kinetics (Kholodenko, 2006). Therefore, inhibition of any kinase, X_1, X_2, …, X_{n-1} or the output T (over a threshold value) will lead to incomplete reactivation and the steady-state T value will remain below its pre-inhibition level (Figures 3E and S2E, blue and orange curves). For the network in Figure 3F (Equation 7.8) the activation of X_1 by Y_1 is not constrained by the moiety conservation, merely because of unlimited synthesis of X_1^i (Equation 7.8). As a result, this network is capable of complete T reactivation in response to inhibition of X_1 or X_2 (Figures 3G and 3H, blue curves). However, neither signaling network can completely or perfectly reactivate the output signaling if any node downstream of X_2, or the output protein T, or the synthesis of Y_1 is inhibited.

Pathway crosstalk can lead to paradoxical activation by an inhibitor: In a crosstalk example in Figure 4A an upstream kinase X_1 signals to the output protein T through a cascade of kinases (X_i), and also activates the pathway (Y_1, …, Y_M) that inhibits T. The local response of the primary target X_1 to the drug I is defined as,

$$r_{X_1 I} = \left.\frac{\partial X_1}{\partial I}\right|_{tier\, X_1\, steady\, state}$$
$$\Delta X_1 = r_{X_1 I} \cdot \Delta I \,. \qquad \text{(Equation 8.1)}$$

Given that the output T is activated by the kinase cascade (X_1, …, X_N and inhibited through an incoherent feedforward loop by the pathway (Y_1, …, Y_M) that in turn is activated by X_1 (Figure 4A), we can write,

Author Manuscript Author Manuscript Author Manuscript Author Manuscript

$$\Delta T = \left(r_{TX_{N-1}} \cdot r_{X_{N-1}X_{N-2}} \cdot \ldots \cdot r_{X_2x_1} + r_{Y_1X_1} \cdot r_{Y_2Y_1} \ldots \cdot r_{TY_M}\right) \cdot \Delta X_1 = (P_X + P_Y) \cdot \Delta X_1 . \quad \text{(Equation 8.2)}$$

Here P_X and P_Y are the products of the connection coefficients from X_1 and Y_1 to T along the pathways X and Y. Substituting Equation 8.1 in Equation 8.2 and proceeding to the limit of infinitesimal changes, we arrive at Equation 8 of the main text.

To illustrate paradoxical responses to the drug I, we present a model of pathway crosstalk for the example shown in Figure 4A with $N = 2$ and $M = 2$. Kinetics of the pathway components are described by the following equations,

$$\begin{aligned}
\frac{dX_1}{dt} &= \frac{V_{X1a}S\left(X_1^{tot} - X_1\right)}{K_{X1a} + \left(X_1^{tot} - X_1\right)} \cdot \frac{1}{1 + I/K_d^{IX1}} - \frac{V_{X1}X_1}{K_{X1} + X_1} \\
\frac{dX_2}{dt} &= \frac{V_{X2a}X_1\left(X_2^{tot} - X_2\right)}{K_{X2a} + \left(X_2^{tot} - X_2\right)} - \frac{V_{X2}X_2}{K_{X2} + X_2} \\
\frac{dY_1}{dt} &= \frac{V_{Y1a}X_1\left(Y_1^{tot} - Y_1\right)}{K_{Y1a} + \left(Y_1^{tot} - Y_1\right)} - \frac{V_{Y1}Y_1}{K_{Y1} + Y_1} \\
\frac{dY_2}{dt} &= \frac{V_{Y2a}Y_1\left(Y_2^{tot} - Y_2\right)}{K_{Y2a} + \left(Y_2^{tot} - Y_2\right)} - \frac{V_{Y2}Y_2}{K_{Y2} + Y_2} \\
\frac{dT}{dt} &= \frac{V_{Ta}X_2\left(T^{tot} - T\right)}{K_{Ta} + \left(T^{tot} - T\right)} \cdot \frac{1 + \gamma_i Y_2/K_{yi}}{1 + Y_2/K_{yi}} - \frac{V_T T}{K_T + T} .
\end{aligned} \quad \text{(Equation 8.3)}$$

Depending on parameters the dose-response curve in (T, X_1) coordinates can be either convex (Figure 4C) or concave (Figure 4D). The parameters corresponding to convex and concave dose-response curves are presented in Table S1.

Inhibition of a kinase upstream of the point of crosstalk: In the example shown in Figure S3A the crosstalk point is at the 3rd cascade tier rather than at the level of the upstream kinase (X_1) The kinase X_2 is the primary drug target. Its local response to the inhibitor I is denoted as r_{X_2I}. The systems-level response (R_{TI}) of the output T to the drug I that inhibits kinase X_2 is given by,

$$R_{TI} = r_{X_2I} \cdot r_{X_3X_2} \cdot \left(P_{TX_3} + P_Y\right). \quad \text{(Equation 8.4)}$$

Here P_{X_3} is the product of the connection coefficients from the crosstalk kinase X_3 to the output T. Because kinases in the pathway X activate each other and subsequently the output, P_{X_3} is positive and P_Y is negative, because the pathway Y inhibits T.

Thus, if a kinase upstream of branching point is inhibited, the expression for the global response to inhibition contains 2 terms with different signs, similarly to Equation 7 in the main text. Depending on the values of P_{X_3} and P_Y the response to inhibition of X_2 can be either positive or negative, and the dose response curve can be either convex or concave, Figures S3B (see Data S3 for kinetic equations and parameters).

Author Manuscript Author Manuscript Author Manuscript Author Manuscript

Inhibition of a kinase downstream of the point of crosstalk: We now consider a kinase downstream of the point of crosstalk as primary drug target, for instance, X_k, $k > 3$, as illustrated in Figure S3C. The local response $r_{X_k I}$ of X_k to the drug I is defined as,

$$r_{X_k I} = \left.\frac{\partial X_k}{\partial I}\right|_{tier\ X_k\ steady\ state}$$

Then, for the responses of X_k and T to a change in the drug I dose, we can write,

$$\Delta X_k = r_{X_k I} \cdot \Delta I$$
$$\Delta T = P_{T X_k} \cdot \Delta X_k$$

Here, P_{X_k} is the product of the connection coefficients from X_k to the output T,

$$P_{T X_k} = r_{X_k X_{k+1}} \cdot \ldots \cdot r_{X_{N-1} X_N} \cdot r_{X_N X_T} \cdot \quad \text{(Equation 8.5)}$$

By substituting the expression for ΔX_k into ΔT and proceeding to the limit of infinitesimal changes, we obtain the expression of the global response of T, when X_k is the primary drug target,

$$R_{TI} = r_{X_k I} \cdot P_{T X_k} . \quad \text{(Equation 8.6)}$$

Equation 8.6 proves that if the cascade is inhibited below a branching point, then the systems-level response to inhibition will always be negative ruling out paradoxical activation in response to a drug, as illustrated in Figure S3D (see Data S3 for kinetic equations and parameters).

Feedback loops modulate paradoxical inhibitor responses: Consider a signaling cascade presented in Figure 4E. Because the first level kinase X_1 is only affected by a drug (I) and feedback from the output T, we have,

$$\Delta X_1 = r_{X_1 T} \cdot \Delta T + r_{X_1 I} \cdot \Delta I . \quad \text{(Equation 8.7)}$$

The output T is activated by the kinase cascade (X_1, …, X_{N-1}) and inhibited through an incoherent feedforward loop emanating from a pathway (Y_1, …, Y_M) that in turn is activated by X_1. Consequently, we can write,

$$\Delta T = \left(r_{T X_{N-1}} \cdot r_{X_{N-1} X_{N-2}} \cdot \ldots \cdot r_{X_2 X_1} + r_{Y_1 X_1} \cdot r_{Y_2 Y_1} \ldots \cdot r_{T Y_M}\right) \cdot \Delta X_1 = (P_X + P_Y) \cdot \Delta X_1 . \quad \text{(Equation 8.8)}$$

Here P_X and P_Y are the products of the connection coefficients from X_1 and Y_1 to T along the pathways X and Y.

Substituting Equation 8.7 in Equation 8.8 and proceeding to the limit of infinitesimal changes, we arrive at Equation 8 of the main text.

Author Manuscript Author Manuscript Author Manuscript Author Manuscript

To illustrate how feedback modulates paradoxical responses to inhibition, we present a model of the pathways shown in Figure 4E for $N = 2$ and $M = 2$. Kinetics of the pathway components is described by the following equations,

$$\begin{aligned}
\frac{dX_1}{dt} &= \frac{V_{X1a}S\left(X_1^{tot} - X_1\right)}{K_{X1a} + \left(X_1^{tot} - X_1\right)} \cdot \frac{1 + \gamma_T T/K_i}{1 + T/K_i} \cdot \frac{1}{1 + I_{X1}/K_d^{IX1}} - \frac{V_{X1}X_1}{K_{X1} + X_1} \\
\frac{dX_2}{dt} &= \frac{V_{X2a}X_1\left(X_2^{tot} - X_2\right)}{K_{X2a} + \left(X_2^{tot} - X_2\right)} - \frac{V_{X2}X_2}{K_{X2} + X_2} \\
\frac{dY_1}{dt} &= \frac{V_{Y1a}X_1\left(Y_1^{tot} - Y_1\right)}{K_{Y1a} + \left(Y_1^{tot} - Y_1\right)} - \frac{V_{Y1}Y_1}{K_{Y_1} + Y_1} \\
\frac{dY_2}{dt} &= \frac{V_{Y2a}Y_1\left(Y_2^{tot} - Y_2\right)}{K_{Y2a} + \left(Y_2^{tot} - Y_2\right)} - \frac{V_{Y2}Y_2}{K_{Y2} + Y_2} \\
\frac{dT}{dt} &= \frac{V_{Ta}X_2\left(T^{tot} - T\right)}{K_{Ta} + \left(T^{tot} - T\right)} \cdot \frac{1 + \gamma_i Y_2/K_{yi}}{1 + Y_2/K_{yi}} - \frac{V_T T}{K_T + T}.
\end{aligned} \quad \text{(Equation 8.9)}$$

Parameter sets are presented in Table S1. Figures 4F and 4G illustrate how feedback modulates convex dose-response curves and concave dose-response curves.

Next, we analyze responses to the inhibition of a kinase localized inside a feedback loop but upstream of the point of crosstalk. For the pathways shown in Figure S3C, where X_3 is the primary drug target, the changes in X_3, X_1 and T following a change in the drug dose I are the following,

$$\begin{aligned}
\Delta X_1 &= r_{X_1T} \cdot \Delta T \\
\Delta X_3 &= r_{X_2X_1} \cdot r_{X_3X_2} \cdot \Delta X_1 + r_{X_3I}\Delta I \\
\Delta T &= \left(P_{X_3} + P_Y\right) \cdot \Delta X_3 .
\end{aligned} \quad \text{(Equation 8.10)}$$

Solving these equations with respect to ΔT we obtain the following expression for the global response of T to the inhibition of X_3 by the drug I,

$$R_{TI} = \frac{P_{TX_3} + P_Y}{1 - r_{X_1T}r_{X_2X_1}r_{X_3X_2}\left(P_{X_3} + P_Y\right)} \cdot r_{X_3I} . \quad \text{(Equation 8.11)}$$

Equation 8.11 demonstrates that the systems-level response to a drug can be positive or negative depending on the product of the sensitivities P_{TX_3} and P_Y, as illustrated in Figures S3F and S3G (see Data S3 for kinetic equations and parameters).

If the primary drug target, kinase X_k, is downstream of the branching point (Figure S3H), the responses of X_1, X_k and T to inhibition are related as follows,

$$\begin{aligned}
\Delta X_1 &= r_{X_1T} \cdot \Delta T \\
\Delta X_k &= P_{X_kX_1} \cdot \Delta X_1 + r_{X_k} \cdot \Delta I \\
\Delta T &= P_Y \cdot \Delta X_1 + P_{TX_k} \cdot \Delta X_k .
\end{aligned} \quad \text{(Equation 8.12)}$$

Author Manuscript Author Manuscript Author Manuscript Author Manuscript

Here $P_{X_kX_1}$ is the product of the connection coefficients from X_1 to X_k, and P_{TX_k} is the product of the connection coefficients from X_k to T (see Equation 8.5). By solving Equations 8.12 with respect to ΔT, we obtain the following expression for the systems-level response of T to drug inhibition, if X_k is the primary drug target,

$$R_{TI} = \frac{P_{TX_k}}{1 - r_{X_1}r_{X_2X_1}r_{X_3X_2}\left(P_{X_3} + P_Y\right)} \cdot r_{X_kI}\,. \qquad \text{(Equation 8.13)}$$

Equation 8.13 demonstrates that although the feedback connection modulates the systems-level response, it is always negative and cannot change its sign if the primary drug target embraced by the feedback is located downstream of the point of crosstalk. This rules out the possibility of paradoxical pathway activation by an inhibitor of X_k, as illustrated in Figures S3I and S3J (see Data S3 for kinetic equations and parameters)

Network topology where feedforward signal flow incorporates feedback loops: The network diagram shown in Figure S4A includes two non-identical routes of signal flow from the primary drug target X_2 to the output T. To obtain the systems-level response (R_{TI}) of the output T to a drug I we will use Equation 1.9, which is valid for any network topology. The connectivity matrix for this scheme reads as follows,

$$\boldsymbol{r} = \begin{pmatrix} -1 & r_{X_1X_2} & 0 & 0 & 0 \\ r_{X_2X_1} & -1 & 0 & 0 & 0 \\ 0 & r_{X_3X_2} & -1 & 0 & 0 \\ r_{Y_1X_1} & 0 & 0 & -1 & 0 \\ 0 & 0 & r_{TX_3} & r_{TY_1} & -1 \end{pmatrix}. \qquad \text{(Equation 8.14)}$$

The local drug response vector reads as,

$$\boldsymbol{r}_{xI} = \begin{pmatrix} 0 \\ r_{X_2I} \\ 0 \\ 0 \\ 0 \end{pmatrix}. \qquad \text{(Equation 8.15)}$$

Using Equation 1.9 we obtain the following expression for R_{TI},

$$R_{TI} = \frac{r_{TX_3}r_{X_3X_2} + r_{TY_1}r_{X_1X_2}r_{Y_1X_1}}{1 - r_{X_1X_2}r_{X_2X_1}} \cdot r_{X_2I}\,. \qquad \text{(Equation 8.16)}$$

The connectivity coefficients, r_{TX_3} and r_{TY_1}, are both positive, whereas $r_{X_1X_2}$ is negative (Figure S4A). Thus, the expression for R_{TI} has two terms with different signs in the numerator, which is a prerequisite for observing paradoxical drug responses. Negative feedback from X_2 to X_1 is necessary to observe paradoxical drug response.

Author Manuscript Author Manuscript Author Manuscript Author Manuscript

Next, we consider kinetic scheme presented in Figure S4B. The network connectivity matrix for this scheme reads,

$$r = \begin{pmatrix} -1 & 0 & r_{X_1Y_1} & 0 & 0 \\ r_{X_2X_1} & -1 & 0 & 0 & 0 \\ r_{Y_1X_1} & 0 & -1 & 0 & 0 \\ 0 & 0 & r_{Y_2Y_1} & -1 & 0 \\ 0 & r_{TX_2} & 0 & r_{TY_2} & -1 \end{pmatrix}. \quad \text{(Equation 8.17)}$$

The local drug response vector reads as,

$$r_{xI} = \begin{pmatrix} 0 \\ r_{X_1I} \\ 0 \\ 0 \\ 0 \end{pmatrix}. \quad \text{(Equation 8.18)}$$

Using Equation 1.9 we obtain the following expression for R_{TI},

$$R_{TI} = \frac{r_{TX_2}r_{X_2X_1} + r_{TY_2}r_{Y_1x_1}r_{Y_2Y_1}}{1 - r_{X_1Y_1}r_{Y_1X_1}} \cdot r_{X_1I}. \quad \text{(Equation 8.19)}$$

We can readily see that Equations 8.16 and 8.19 are equivalent after the following renaming of nodes, $X_2 \rightarrow X_1$, $X_1 \rightarrow Y_1$, $Y_1 \rightarrow Y_2$, $X_3 \rightarrow X_2$. This equivalence is based on the topological equivalence of the signaling networks shown in Figures S4A and S4B. For a signaling network that is affected by a drug (I), the number of the separate products in the nominator of the systems-level response R_{TI} gives the number of routes connecting the primary drug target with the pathway output T. The dose responses of these two equivalent networks are clearly identical and are illustrated in Figures S4C and S4D (see Data S4 for kinetic equations and parameters).

Opposite drug responses emerging at hysteresis branches: If there are two or more activating and inhibiting connection routes from the primary drug target to the output kinase coupled with intertwined feedback loops that lead to bistability, drug responses can exhibit hysteresis and behave differently at different hysteresis branches. An illustrative example is shown in Figures S5A and S5B. At a point of crosstalk, signaling protein X_2 activates downstream proteins X_3 and Y_1, one of which (X_3) inhibits the common output T, whereas the other (Y_1) activates it. In turn, T inhibits X_2 via positive feedback to the upstream kinase X_1 that is a primary drug target. This positive feedback is a prerequisite for bistability and hysteresis in the pathway. X_2 is inhibited by X_1 and activated by positive feedback from Y_1, Figure S5A. In contrast to a chain of kinases activating each other, here two inhibitory connections from the kinase X_1 contribute to the output T activation. The kinetic diagram in Figure S5A resembles the Rac1-RhoA GTPase network where Rac1 (T) activates the kinase PAK (X_1) that inhibits RhoA (X_2), which, in turn, activates Rac1 via DIA (Y_1) and inhibits Rac1 via

Author Manuscript Author Manuscript Author Manuscript Author Manuscript

the kinase ROCK (X_3). Under specific conditions, the Rac1-RhoA GTPase network can exhibit bistability and hysteresis (Bolado-Carrancio et al., 2020).

Suppose the sensitivity of the output T to the inhibition of the crosstalk kinase X_2 is greater for the connection route via the kinase X_3 that inhibits T than for the route via the protein Y_1 that activates T. Then, the inhibitor (I) of X_1 that in turn inhibits X_2 will activate T. As shown by an arrow that indicates the system trajectory along the solid black curve in Figure S5B, T is activated by a drug that inhibits X_1. When the drug dose reaches a threshold value (the bifurcation point), the system flips from this stable state to another stable state. This abrupt switch to the greatly higher activity is shown by the arrow 'Go up' along a black dotted line that leads to the red line formed by alternative steady states. If the drug dose decreases, while the system is in the high activity state, the output activity increases, as shown by a red arrow along the red hysteresis curve in Figure S5B. This response to the drug is different from the response observed for the low activity branch where the response decreases with the decrease in the drug dose (solid black curve in Figure S5B). With the further decrease in drug doses, the low threshold is reached, and the system abruptly switches to the low activity as shown by the arrow 'Go down' along a red dotted line leading to the solid black line of stable steady states in Figure S5B. These network trajectories illustrate a hysteretic drug response, a feature of bistable systems (Kholodenko, 2006).

The dynamics of species presented in Figure S5A are governed by the following equations,

$$\begin{aligned}
\frac{dX_1}{dt} &= V_{X_1a}\frac{1+\gamma_T^{X_1}X_1/K_T^{X_1}}{1+X_1/K_T^{X_1}}\frac{\left(X_1^{tot}-X_1\right)/\left(K_{X_1a}(1+I/K_d)\right)}{1+\left(X_1^{tot}-X_1\right)/\left(K_{X_1a}(1+I/K_d)\right)} - V_{X_1}\frac{X_1/K_{X_1}}{1+X_1/K_{X_1}}\\
\frac{dX_2}{dt} &= V_{X_2a}\frac{1+\gamma_{Y_1}^{X_2}Y_1/K_{Y_1}^{X_2}}{1+Y_1/K_{Y_1}^{X_2}}\frac{1+\gamma_{X_1}^{X_2}X_1/K_{X_1}^{X_2}}{1+X_1/K_{X_1}^{X_2}}\frac{\left(X_2^{tot}-X_2\right)/K_{X_2}}{1+\left(X_2^{tot}-X_2\right)/K_{X_2}} - V_{X_2}\frac{X_2/K_{X_2}}{1+X_2/K_{X_2}}\\
\frac{dX_3}{dt} &= V_{X_3a}\frac{1+\gamma_{X_2}^{X_3}X_2/K_{X_2}^{X_3}}{1+X_2/K_{X_2}^{X_3}}\frac{\left(X_3^{tot}-X_3\right)/K_{X_3a}}{1+\left(X_3^{tot}-X_3\right)/K_{X_3a}} - V_{X_3}\frac{X_3/K_{X_3}}{1+X_3/K_{X_3}}\\
\frac{dY_1}{dt} &= V_{Y_1}\frac{1+\gamma_{X_2}^{Y_1}X_2/K_{X_2}^{Y_1}}{1+X_2/K_{X_2}^{Y_1}}\frac{\left(Y_1^{tot}-Y_1\right)/K_{Y_1a}}{1+\left(Y_1^{tot}-Y_1\right)/K_{Y_1a}} - V_{Y_1}\frac{Y_1/K_{Y_1}}{1+Y_1/K_{Y_1}}\\
\frac{dT}{dt} &= V_{Ta}\frac{1+\gamma_{Y_1}^{T}Y_1/K_{Y_1}^{T}}{1+Y_1/K_{Y_1}^{T}}\frac{\left(T^{tot}-T\right)/K_{Ta}}{1+\left(T^{tot}-T\right)/K_{Ta}}\\
&- V_T\frac{1+\gamma_{X_3}^{T}X_3/K_{X_3}^{T}}{1+X_3/K_{X_3}^{T}}\frac{T/K_T}{1+T/K_T}
\end{aligned}$$

(Equation 8.20)

.

The steady-state trajectories shown in Figure S5B are obtained using Equation 8.20 with parameters listed in Table S1.

Paradoxical drug responses in pathways with multiple output proteins: Consider a signaling cascade presented in Figure S5C. Response of the first output T_1 to the drug reads,

$$\Delta T_1 = r_{T_1 I}\cdot \Delta I\,. \qquad \text{(Equation 9.1)}$$

Because the first level kinase X_1 is only affected by a feedback from the output T_1, we have,

Author Manuscript Author Manuscript Author Manuscript Author Manuscript

$$\Delta X_1 = r_{X_1T_1} \cdot \Delta T_1 . \quad \text{(Equation 9.2)}$$

The second output T_2 is activated by the kinase cascade (X_1, Y_1 …, Y_M). Consequently, we can write,

$$\Delta T_2 = \left(r_{T_2Y_M} \cdot r_{Y_MY_{M-1}} \cdot \ldots \cdot r_{Y_2Y_1} \cdot r_{Y_1X_1}\right) \cdot \Delta X_1 = P_Y \cdot \Delta X_1 . \quad \text{(Equation 9.3)}$$

Here, P_Y is the product of the connection coefficients from X_1 to T_2 along the pathway Y. Substituting Equations 9.1 and 9.2 into Equation 9.3 and proceeding to the limit of infinitesimal changes, we arrive at the following expression for R_{T_2I},

$$R_{T_2I} = P_Y \cdot r_{X_1T_1} \cdot r_{T_1I} . \quad \text{(Equation 9.4)}$$

$P_Y > 0$ because X_1 activates T_2 via pathway Y, $r_{X_1T_1} < 0$ because the feedback is negative, and $r_{T_1I} < 0$ because inhibitor inhibits T_1. Therefore, $r_{T_2I} > 0$, i.e., inhibitor activates T_2.

To illustrate the response of T_2 to inhibition of T_1, we present the following model for $N = 2$ and $M = 1$ (Figure S5C),

$$\begin{aligned}
\frac{dX_1}{dt} &= \frac{V_{X1a}S\left(X_1^{tot} - X_1\right)}{K_{X1a} + \left(X_1^{tot} - X_1\right)} \cdot \frac{1 + \gamma_{T_1}T_1/K_i}{1 + T_1/K_i} - \frac{V_{X1}X_1}{K_{X_1} + X_1} \\
\frac{dX_2}{dt} &= \frac{V_{X2a}X_1\left(X_2^{tot} - X_2\right)}{K_{X2a} + \left(X_2^{tot} - X_2\right)} - \frac{V_{X2}X_2}{K_{X2} + X_2} \\
\frac{dT_1}{dt} &= \frac{V_{T_1a}X_2\left(T_1^{tot} - T_1\right)}{K_{T_1a} + \left(T_1^{tot} - T_1\right)} \cdot \frac{1}{1 + I/K_d} - \frac{V_{T_1}T_1}{K_{T_1} + T_1} \\
\frac{dY_1}{dt} &= \frac{V_{Y1a}X_1\left(Y_1^{tot} - Y_1\right)}{K_{Y_1a} + \left(Y_1^{tot} - Y_1\right)} - \frac{V_{Y_1}Y_1}{K_{Y_1} + Y_1} \\
\frac{dT_2}{dt} &= \frac{V_{T_2a}Y_1\left(T_2^{tot} - T_2\right)}{K_{T_2a} + \left(T_2^{tot} - T_2\right)} - \frac{V_{T_2}T_2}{K_{T_2} + T_2} .
\end{aligned} \quad \text{(Equation 9.5)}$$

Model parameters are presented in Table S1.

Figure S5E illustrates the case when T_1 has both negative and positive connections to the kinases upstream of a branching point. In this case responses of T_1 and X_1 are described by Equations 9.1 and 9.2 as well. For the response of X_2 we have,

$$\Delta X_2 = r_{X_2X_1} \cdot \Delta X_1 + r_{X_2T_1} \cdot \Delta T_1 . \quad \text{(Equation 9.6)}$$

For the response of the second output T_2 we can write,

$$\Delta T_2 = \left(r_{T_2Y_M} \cdot r_{Y_MY_{M-1}} \cdot \ldots \cdot r_{Y_2Y_1} \cdot r_{Y_1X_2}\right) \cdot \Delta X_2 = P_Y \cdot \Delta X_2 . \quad \text{(Equation 9.7)}$$

Author Manuscript Author Manuscript Author Manuscript Author Manuscript

Here P_Y is the product of the connection coefficients from X_2 to T_2 along the pathway Y. Substituting Equations 9.1, 9.2, and 9.6 in Equation 9.7, we arrive at the following expression for R_{T_2I},

$$R_{T_2I} = P_Y \cdot \left(r_{X_1T_1} \cdot r_{X_2x_1} + r_{X_2T_1}\right) \cdot r_{T_1I}\,. \qquad \text{(Equation 9.8)}$$

Since $r_{X_1T_1} \cdot r_{X_2X_1} > 0$ and $r_{X_2T_1}$, R_{T_2I} can be either positive or negative depending on parameters. Consequently, the dose response curve for T_2 can be either convex or concave. This conclusion is illustrated by the following model with $N = 2$ and $M = 1$,

$$\begin{aligned}
\frac{dX_1}{dt} &= \frac{V_{X1a}S\left(X_1^{tot} - X_1\right)}{K_{X1a} + \left(X_1^{tot} - X_1\right)} \cdot \frac{1 + \gamma_{T_1}^{X_1} T_1/K_{i1}}{1 + T_1/K_{i1}} - \frac{V_{X1}X_1}{K_{X1} + X_1} \\
\frac{dX_2}{dt} &= \frac{V_{X2a}X_1\left(X_2^{tot} - X_2\right)}{K_{X2a} + \left(X_2^{tot} - X_2\right)} \cdot \frac{1 + \gamma_{T_1}^{X_2} T_1/K_{i2}}{1 + T_1/K_{i2}} - \frac{V_{X2}X_2}{K_{X2} + X_2} \\
\frac{dT_1}{dt} &= \frac{V_{T_1a}X_2\left(T_1^{tot} - T_1\right)}{K_{T_1a} + \left(T_1^{tot} - T_1\right)} \cdot \frac{1}{1 + I/K_d} - \frac{V_{T_1}T_1}{K_{T_1} + T_1} \\
\frac{dY_1}{dt} &= \frac{V_{Y1a}X_2\left(Y_1^{tot} - Y_1\right)}{K_{Y1a} + \left(Y_1^{tot} - Y_1\right)} - \frac{V_{Y1}Y_1}{K_{Y1} + Y_1} \\
\frac{dT_2}{dt} &= \frac{V_{T_2a}Y_1\left(T_2^{tot} - T_2\right)}{K_{T_2a} + \left(T_2^{tot} - T_2\right)} - \frac{V_{T_2}T_2}{K_{T_2} + T_2}\,.
\end{aligned} \qquad \text{(Equation 9.9)}$$

Model parameters yielding concave and convex dose response curves (see Figures S5F and S5G) are presented in Table S1.

Mechanistic models of the RAS/RAF/MEK/ERK pathway and inhibitor treatments: The rule-based model of RAS/RAF/MEK/ERK pathway developed previously (Rukhlenko et al., 2018) was extended to explicitly include SOS, RAS and the inhibitory phosphorylation of SOS by active ERK. The resulting model has 573 rules that generate 2043 species and 15613 reactions. Our model integrates the structural properties and regulatory dynamics of RAF isoforms with thermodynamic and conformation analyses of inhibitor-target interactions. It employs a rule-based, domain-oriented approach, which explicitly monitors the conformational and phosphorylation states of multiple pathway proteins, including inhibiting and activating phosphosites (Borisov et al., 2008; Chylek et al., 2014; Varga et al., 2017). Featuring negative feedback loops from ERK to BRAF, CRAF and a main RAS activator, the guanine exchange factor SOS (Figure 5A), the model reliably predicts the ERK pathway responses to RAF and MEK inhibitors and their combinations for cells with different genetic background, as validated in previous experiments (Rukhlenko et al., 2018).

The reaction laws, equations and the rate and dissociation constants are given in Data S5 in SBML format.

Author Manuscript Author Manuscript Author Manuscript Author Manuscript

The time courses of the ERK activity responses were calculated for type I½ RAF inhibitors, which induced (Figure 5B) or did not induce (Figure 5C) RAF dimerization at the doses equal to 150 K_d.

To assess effects of inhibitor combinations on ERK signaling we calculated stationary ppERK responses across a two-dimensional plane of drug doses (Figures 5D, 5E, 6A, and 6B). Lines of constant ppERK inhibition are termed Loewe isoboles. A drug dose that inhibits the basal ERK activity by 50% is known as IC_{50} dose. In general, ICZ drug dose corresponds to ppERK inhibition by Z%.

The change in RTK activities from low to high levels in cells expressing WT RAS and BRAFV600E/WT (Figures 5D and 5E, respectively) was modeled as follows. The equilibrium constant of SOS binding to RTK-GRB2 complexes was increased 5-fold (*cf.* the values of the SOS membrane-cytoplasm distribution parameter kSOStransl in the files "RAS_to_ERK_BRAFV600E_ lowRTK_sbml.xml" and "RAS_to_ERK_BRAFV600E_highRTK_sbml.xml" of Data S5). To simulate WT BRAF and oncogenic RAS mutant conditions (Figures 6A and 6B) the rate constant of the RAS-GAP activity was decreased 10-fold (*cf.* the values of the parameter V_RASGAP in the files "RAS_to_ERK_BRAFV600E_lowRTK_sbml.xml" and "RAS_to_ERK_WTRAF_oncoRAS_sbml.xml" of Data S5). These parameter changes resulted in the stationary RAS-GTP levels equal to ~25 nM in WT RAS cells with low RTK activity, ~100 nM in WT RAS cells with high RTK activity, and ~250 nM in cells with low RTK activity and oncogenic RAS. The total RAS concentration was 750 nM.

Inhibitor induced dimerization was described by the ratio of the dimerization constant for the complex of inhibitor-bound RAF monomer and free RAF monomer and the dimerization constant for the complex of two free RAF monomers (Kholodenko, 2015). This ratio is termed the facilitation factor (f), and an f smaller than 1 corresponds to the facilitation of RAF dimerization by the inhibitor. The factor f for a paradox breaker Type I½ RAF inhibitor was modeled by a 10-fold increase in the f value for a typical Type I½ RAF inhibitor (Figure S8). The effect of 14-3-3 overexpression was modeled by a 2-fold reduction in the dissociation constants of RAF dimers at the physiological abundance of 14-3-3 proteins.

QUANTIFICATION AND STATISTICAL ANALYSIS

Western Blots were quantified using ImageJ software (Schindelin et al., 2012). All measurements, both Western Blot and MESOSCALE, were done in 3 replicates, if not specified otherwise in the respective figure legends. Error bars represent standard error of mean. To estimate statistical significance and calculate p values, unpaired t test was used. To assess drug synergy effects, Talalay-Chou combination index (Chou, 2010) and Loewe isoboles (Greco et al., 1995) were used.

Supplementary Material

Refer to Web version on PubMed Central for supplementary material.

Author Manuscript Author Manuscript Author Manuscript Author Manuscript

ACKNOWLEDGMENTS

We thank Prof. Bond for the OCI-AML-3 cells. This work was supported by NIH/NCI grant R01CA244660, EU NanoCommons grant 731032, and Science Foundation Ireland grants 18/SPP/3522 and 14/IA/2395.

REFERENCES

Aleksakhina SN, Kashyap A, and Imyanitov EN (2019). Mechanisms of acquired tumor drug resistance. Biochim. Biophys. Acta Rev. Cancer 1872, 188310. [PubMed: 31442474]

Alexander PB, and Wang XF (2015). Resistance to receptor tyrosine kinase inhibition in cancer: molecular mechanisms and therapeutic strategies. Front. Med 9, 134–138. [PubMed: 25957263]

Amit I, Citri A, Shay T, Lu Y, Katz M, Zhang F, Tarcic G, Siwak D, Lahad J, Jacob-Hirsch J, et al. (2007). A module of negative feedback regulators defines growth factor signaling. Nat. Genet 39, 503–512. [PubMed: 17322878]

Aoki SK, Lillacci G, Gupta A, Baumschlager A, Schweingruber D, and Khammash M (2019). A universal biomolecular integral feedback controller for robust perfect adaptation. Nature 570, 533–537. [PubMed: 31217585]

Aronson BD, Johnson KA, Loros JJ, and Dunlap JC (1994). Negative feedback defining a circadian clock: autoregulation of the clock gene frequency. Science 263, 1578–1584. [PubMed: 8128244]

Bakshi UA, and Goyal SC (2007). Control Systems Engineering (Technical Publications).

Baljuls A, Kholodenko BN, and Kolch W (2013). It takes two to tango–signalling by dimeric Raf kinases. Mol. Biosyst 9, 551–558. [PubMed: 23212737]

Bastiaens P, Birtwistle MR, Blüthgen N, Bruggeman FJ, Cho KH, Cosentino C, de la Fuente A, Hoek JB, Kiyatkin A, Klamt S, et al. (2015). Silence on the relevant literature and errors in implementation. Nat. Biotechnol 33, 336–339. [PubMed: 25850052]

Bennett S (1996). A brief history of automatic control. IEEE Contr. Syst. Mag 16, 17–25.

Bessman NJ, Bagchi A, Ferguson KM, and Lemmon MA (2014). Complex relationship between ligand binding and dimerization in the epidermal growth factor receptor. Cell Rep. 9, 1306–1317. [PubMed: 25453753]

Blaževitš O, Mideksa YG, Šolman M, Ligabue A, Ariotti N, Nakhaeizadeh H, Fansa EK, Papageorgiou AC, Wittinghofer A, Ahmadian MR, and Abankwa D (2016). Galectin-1 dimers can scaffold Raf-effectors to increase H-ras nanoclustering. Sci. Rep 6, 24165. [PubMed: 27087647]

Bolado-Carrancio A, Rukhlenko OS, Nikonova E, Tsyganov MA, Wheeler A, Garcia-Munoz A, Kolch W, von Kriegsheim A, and Kholodenko BN (2020). Periodic propagating waves coordinate RhoGTPase network dynamics at the leading and trailing edges during cell migration. eLife 9, e58165. [PubMed: 32705984]

Boned Del Río I, Young LC, Sari S, Jones GG, Ringham-Terry B, Hartig N, Rejnowicz E, Lei W, Bhamra A, Surinova S, and Rodriguez-Viciana P (2019). SHOC2 complex-driven RAF dimerization selectively contributes to ERK pathway dynamics. Proc. Natl. Acad. Sci. USA 116, 13330–13339. [PubMed: 31213532]

Borisov NM, Chistopolsky AS, Faeder JR, and Kholodenko BN (2008). Domain-oriented reduction of rule-based network models. IET Syst. Biol 2, 342–351. [PubMed: 19045829]

Boutros T, Chevet E, and Metrakos P (2008). Mitogen-activated protein (MAP) kinase/MAP kinase phosphatase regulation: roles in cell growth, death, and cancer. Pharmacol. Rev 60, 261–310. [PubMed: 18922965]

Briat C, Gupta A, and Khammash M (2016). Antithetic Integral Feedback Ensures Robust Perfect Adaptation in Noisy Biomolecular Networks. Cell Syst. 2, 15–26. [PubMed: 27136686]

Brown GC, Hoek JB, and Kholodenko BN (1997). Why do protein kinase cascades have more than one level? Trends Biochem. Sci 22, 288.

Bruggeman FJ, Westerhoff HV, Hoek JB, and Kholodenko BN (2002). Modular response analysis of cellular regulatory networks. J. Theor. Biol 218, 507–520. [PubMed: 12384053]

Caunt CJ, and Keyse SM (2013). Dual-specificity MAP kinase phosphatases (MKPs): shaping the outcome of MAP kinase signalling. FEBS J. 280, 489–504. [PubMed: 22812510]

Author Manuscript Author Manuscript Author Manuscript Author Manuscript

Chandarlapaty S, Sawai A, Scaltriti M, Rodrik-Outmezguine V, Grbovic-Huezo O, Serra V, Majumder PK, Baselga J, and Rosen N (2011). AKT inhibition relieves feedback suppression of receptor tyrosine kinase expression and activity. Cancer Cell 19, 58–71. [PubMed: 21215704]

Chou TC (2010). Drug combination studies and their synergy quantification using the Chou-Talalay method. Cancer Res. 70, 440–446. [PubMed: 20068163]

Chylek LA, Harris LA, Tung CS, Faeder JR, Lopez CF, and Hlavacek WS (2014). Rule-based modeling: a computational approach for studying biomolecular site dynamics in cell signaling systems. Wiley Interdiscip. Rev. Syst. Biol. Med 6, 13–36. [PubMed: 24123887]

Corcoran RB, Atreya CE, Falchook GS, Kwak EL, Ryan DP, Bendell JC, Hamid O, Messersmith WA, Daud A, Kurzrock R, et al. (2015). Combined BRAF and MEK Inhibition With Dabrafenib and Trametinib in BRAF V600-Mutant Colorectal Cancer. J. Clin. Oncol 33, 4023–4031. [PubMed: 26392102]

Dey M, Cao C, Dar AC, Tamura T, Ozato K, Sicheri F, and Dever TE (2005). Mechanistic link between PKR dimerization, autophosphorylation, and eIF2alpha substrate recognition. Cell 122, 901–913. [PubMed: 16179259]

Dibrov BF, Zhabotinsky AM, and Kholodenko BN (1982). Dynamic stability of steady states and static stabilization in unbranched metabolic pathways. J. Math. Biol 15, 51–63. [PubMed: 7142835]

Ercan D, Xu C, Yanagita M, Monast CS, Pratilas CA, Montero J, Butaney M, Shimamura T, Sholl L, Ivanova EV, et al. (2012). Reactivation of ERK signaling causes resistance to EGFR kinase inhibitors. Cancer Discov. 2, 934–947. [PubMed: 22961667]

Feillet C, van der Horst GT, Levi F, Rand DA, and Delaunay F (2015). Coupling between the Circadian Clock and Cell Cycle Oscillators: Implication for Healthy Cells and Malignant Growth. Front. Neurol 6, 96. [PubMed: 26029155]

Ferrell JE Jr. (1997). How responses get more switch-like as you move down a protein kinase cascade. Trends Biochem. Sci 22, 288–289.

Fey D, Croucher DR, Kolch W, and Kholodenko BN (2012). Crosstalk and signaling switches in mitogen-activated protein kinase cascades. Front. Physiol 3, 355. [PubMed: 23060802]

Fey D, Halasz M, Dreidax D, Kennedy SP, Hastings JF, Rauch N, Munoz AG, Pilkington R, Fischer M, Westermann F, et al. (2015). Signaling pathway models as biomarkers: patient-specific simulations of JNK activity predict the survival of neuroblastoma patients. Sci. Signal 8, ra130. [PubMed: 26696630]

Frank MJ, Dawson DW, Bensinger SJ, Hong JS, Knosp WM, Xu L, Balatoni CE, Allen EL, Shen RR, Bar-Sagi D, et al. (2009). Expression of sprouty2 inhibits B-cell proliferation and is epigenetically silenced in mouse and human B-cell lymphomas. Blood 113, 2478–2487. [PubMed: 19147787]

Gerosa L, Chidley C, Fröhlich F, Sanchez G, Lim SK, Muhlich J, Chen J-Y, Vallabhaneni S, Baker GJ, Schapiro D, et al. (2020). Receptor-Driven ERK Pulses Reconfigure MAPK Signaling and Enable Persistence of Drug-Adapted BRAF-Mutant Melanoma Cells. Cell Syst. 11, 478–494.e9. [PubMed: 33113355]

Goldbeter A (1995). A model for circadian oscillations in the Drosophila period protein (PER). Proc. Biol. Sci 261, 319–324. [PubMed: 8587874]

Goyal Y, Jindal GA, Pelliccia JL, Yamaya K, Yeung E, Futran AS, Burdine RD, Schüpbach T, and Shvartsman SY (2017). Divergent effects of intrinsically active MEK variants on developmental Ras signaling. Nat. Genet 49, 465–469. [PubMed: 28166211]

Greco WR, Bravo G, and Parsons JC (1995). The search for synergy: a critical review from a response surface perspective. Pharmacol. Rev 47, 331–385. [PubMed: 7568331]

Grob JJ, Amonkar MM, Karaszewska B, Schachter J, Dummer R, Mackiewicz A, Stroyakovskiy D, Drucis K, Grange F, Chiarion-Sileni V, et al. (2015). Comparison of dabrafenib and trametinib combination therapy with vemurafenib monotherapy on health-related quality of life in patients with unresectable or metastatic cutaneous BRAF Val600-mutation-positive melanoma (COMBI-v): results of a phase 3, open-label, randomised trial. Lancet Oncol. 16, 1389–1398. [PubMed: 26433819]

Halasz M, Kholodenko BN, Kolch W, and Santra T (2016). Integrating network reconstruction with mechanistic modeling to predict cancer therapies. Sci. Signal 9, ra114. [PubMed: 27879396]

Author Manuscript Author Manuscript Author Manuscript Author Manuscript

Haling JR, Sudhamsu J, Yen I, Sideris S, Sandoval W, Phung W, Bravo BJ, Giannetti AM, Peck A, Masselot A, et al. (2014). Structure of the BRAF-MEK complex reveals a kinase activity independent role for BRAF in MAPK signaling. Cancer Cell 26, 402–413. [PubMed: 25155755]

Hall-Jackson CA, Goedert M, Hedge P, and Cohen P (1999). Effect of SB 203580 on the activity of c-Raf in vitro and in vivo. Oncogene 18, 2047–2054. [PubMed: 10321729]

Hatzivassiliou G, Song K, Yen I, Brandhuber BJ, Anderson DJ, Alvarado R, Ludlam MJ, Stokoe D, Gloor SL, Vigers G, et al. (2010). RAF inhibitors prime wild-type RAF to activate the MAPK pathway and enhance growth. Nature 464, 431–435. [PubMed: 20130576]

Heidorn SJ, Milagre C, Whittaker S, Nourry A, Niculescu-Duvas I, Dhomen N, Hussain J, Reis-Filho JS, Springer CJ, Pritchard C, and Marais R (2010). Kinase-dead BRAF and oncogenic RAS cooperate to drive tumor progression through CRAF. Cell 140, 209–221. [PubMed: 20141835]

Hu J, Stites EC, Yu H, Germino EA, Meharena HS, Stork PJS, Kornev AP, Taylor SS, and Shaw AS (2013). Allosteric activation of functionally asymmetric RAF kinase dimers. Cell 154, 1036–1046. [PubMed: 23993095]

Huang H, Zeqiraj E, Dong B, Jha BK, Duffy NM, Orlicky S, Thevakumaran N, Talukdar M, Pillon MC, Ceccarelli DF, et al. (2014). Dimeric structure of pseudokinase RNase L bound to 2–5A reveals a basis for interferon-induced antiviral activity. Mol. Cell 53, 221–234. [PubMed: 24462203]

Ishii N, Harada N, Joseph EW, Ohara K, Miura T, Sakamoto H, Matsuda Y, Tomii Y, Tachibana-Kondo Y, Iikura H, et al. (2013). Enhanced inhibition of ERK signaling by a novel allosteric MEK inhibitor, CH5126766, that suppresses feedback reactivation of RAF activity. Cancer Res. 73, 4050–4060. [PubMed: 23667175]

Johnson DB, Menzies AM, Zimmer L, Eroglu Z, Ye F, Zhao S, Rizos H, Sucker A, Scolyer RA, Gutzmer R, et al. (2015). Acquired BRAF inhibitor resistance: a multicenter meta-analysis of the spectrum and frequencies, clinical behaviour, and phenotypic associations of resistance mechanisms. Eur. J. Cancer 51, 2792–2799. [PubMed: 26608120]

Jones DS, Jenney AP, Joughin BA, Sorger PK, and Lauffenburger DA (2018). Inflammatory but not mitogenic contexts prime synovial fibroblasts for compensatory signaling responses to p38 inhibition. Sci. Signal 11, eaal1601. [PubMed: 29511118]

Junttila MR, Li SP, and Westermarck J (2008). Phosphatase-mediated crosstalk between MAPK signaling pathways in the regulation of cell survival. FASEB J. 22, 954–965. [PubMed: 18039929]

Kaimachnikov NP, and Kholodenko BN (2009). Toggle switches, pulses and oscillations are intrinsic properties of the Src activation/deactivation cycle. FEBS J. 276, 4102–4118. [PubMed: 19627364]

Karoulia Z, Wu Y, Ahmed TA, Xin Q, Bollard J, Krepler C, Wu X, Zhang C, Bollag G, Herlyn M, et al. (2016). An Integrated Model of RAF Inhibitor Action Predicts Inhibitor Activity against Oncogenic BRAF Signaling. Cancer Cell 30, 501–503.

Keith CT, Borisy AA, and Stockwell BR (2005). Multicomponent therapeutics for networked systems. Nat. Rev. Drug Discov 4, 71–78. [PubMed: 15688074]

Khan ZM, Real AM, Marsiglia WM, Chow A, Duffy ME, Yerabolu JR, Scopton AP, and Dar AC (2020). Structural basis for the action of the drug trametinib at KSR-bound MEK. Nature 588, 509–514. [PubMed: 32927473]

Kholodenko BN (2000). Negative feedback and ultrasensitivity can bring about oscillations in the mitogen-activated protein kinase cascades. Eur. J. Biochem 267, 1583–1588. [PubMed: 10712587]

Kholodenko BN (2006). Cell-signalling dynamics in time and space. Nat. Rev. Mol. Cell Biol 7, 165–176. [PubMed: 16482094]

Kholodenko BN (2007). Untangling the signalling wires. Nat. Cell Biol 9, 247–249. [PubMed: 17330115]

Kholodenko BN (2015). Drug resistance resulting from kinase dimerization is rationalized by thermodynamic factors describing allosteric inhibitor effects. Cell Rep. 12, 1939–1949. [PubMed: 26344764]

Kholodenko BN, and Westerhoff HV (1995). The macroworld versus the microworld of biochemical regulation and control. Trends Biochem. Sci 20, 52–54. [PubMed: 7701560]

Kholodenko BN, Hoek JB, Westerhoff HV, and Brown GC (1997). Quantification of information transfer via cellular signal transduction pathways. FEBS Lett. 414, 430–434. [PubMed: 9315734]

Author Manuscript Author Manuscript Author Manuscript Author Manuscript

Kholodenko BN, Kiyatkin A, Bruggeman FJ, Sontag E, Westerhoff HV, and Hoek JB (2002). Untangling the wires: a strategy to trace functional interactions in signaling and gene networks. Proc. Natl. Acad. Sci. USA 99, 12841–12846. [PubMed: 12242336]

Klinger B, and Blüthgen N (2014). Consequences of feedback in signal transduction for targeted therapies. Biochem. Soc. Trans 42, 770–775. [PubMed: 25109956]

Klinger B, Sieber A, Fritsche-Guenther R, Witzel F, Berry L, Schumacher D, Yan Y, Durek P, Merchant M, Schäfer R, et al. (2013). Network quantification of EGFR signaling unveils potential for targeted combination therapy. Mol. Syst. Biol 9, 673. [PubMed: 23752269]

Kolch W, Halasz M, Granovskaya M, and Kholodenko BN (2015). The dynamic control of signal transduction networks in cancer cells. Nat. Rev. Cancer 15, 515–527. [PubMed: 26289315]

Kopetz S, Grothey A, Yaeger R, Van Cutsem E, Desai J, Yoshino T, Wasan H, Ciardiello F, Loupakis F, Hong YS, et al. (2019). Encorafenib, Binimetinib, and Cetuximab in *BRAF* V600E-Mutated Colorectal Cancer. N. Engl. J. Med 381, 1632–1643. [PubMed: 31566309]

Koppikar P, Bhagwat N, Kilpivaara O, Manshouri T, Adli M, Hricik T, Liu F, Saunders LM, Mullally A, Abdel-Wahab O, et al. (2012). Heterodimeric JAK-STAT activation as a mechanism of persistence to JAK2 inhibitor therapy. Nature 489, 155–159. [PubMed: 22820254]

Kuznetsov IUA (2004). Elements of Applied Bifurcation Theory, Third Edition (Springer).

Lake D, Corrêa SA, and Müller J (2016). Negative feedback regulation of the ERK1/2 MAPK pathway. Cell. Mol. Life Sci 73, 4397–4413. [PubMed: 27342992]

Larkin J, Ascierto PA, Dréno B, Atkinson V, Liszkay G, Maio M, Mandalà M, Demidov L, Stroyakovskiy D, Thomas L, et al. (2014). Combined vemurafenib and cobimetinib in BRAF-mutated melanoma. N. Engl. J. Med 371, 1867–1876. [PubMed: 25265494]

Lee S, Rauch J, and Kolch W (2020). Targeting MAPK Signaling in Cancer: Mechanisms of Drug Resistance and Sensitivity. Int. J. Mol. Sci 21, 1102.

Lill D, Rukhlenko OS, Mc Elwee AJ, Kashdan E, Timmer J, and Kholodenko BN (2019). Mapping connections in signaling networks with ambiguous modularity. NPJ Syst. Biol. Appl 5, 19. [PubMed: 31149348]

Lito P, Pratilas CA, Joseph EW, Tadi M, Halilovic E, Zubrowski M, Huang A, Wong WL, Callahan MK, Merghoub T, et al. (2012). Relief of profound feedback inhibition of mitogenic signaling by RAF inhibitors attenuates their activity in BRAFV600E melanomas. Cancer Cell 22, 668–682. [PubMed: 23153539]

Mangan S, and Alon U (2003). Structure and function of the feed-forward loop network motif. Proc. Natl. Acad. Sci. USA 100, 11980–11985. [PubMed: 14530388]

Mendiratta G, McFall T, and Stites EC (2019). RAF autoinhibition and 14-3-3 proteins promote paradoxical activation. bioRxiv. 10.1101/849489.

Milewska M, Romano D, Herrero A, Guerriero ML, Birtwistle M, Quehenberger F, Hatzl S, Kholodenko BN, Segatto O, Kolch W, and Zebisch A (2015). Mitogen-Inducible Gene-6 Mediates Feedback Inhibition from Mutated BRAF towards the Epidermal Growth Factor Receptor and Thereby Limits Malignant Transformation. PLoS ONE 10, e0129859. [PubMed: 26065894]

Mina M, Magi S, Jurman G, Itoh M, Kawaji H, Lassmann T, Arner E, Forrest ARR, Carninci P, Hayashizaki Y, et al.; FANTOM Consortium (2015). Promoter-level expression clustering identifies time development of transcriptional regulatory cascades initiated by ErbB receptors in breast cancer cells. Sci. Rep 5, 11999. [PubMed: 26179713]

Montero-Conde C, Ruiz-Llorente S, Dominguez JM, Knauf JA, Viale A, Sherman EJ, Ryder M, Ghossein RA, Rosen N, and Fagin JA (2013). Relief of feedback inhibition of HER3 transcription by RAF and MEK inhibitors attenuates their antitumor effects in BRAF-mutant thyroid carcinomas. Cancer Discov. 3, 520–533. [PubMed: 23365119]

Mukherjee R, Vanaja KG, Boyer JA, Gadal S, Solomon H, Chandarlapaty S, Levchenko A, and Rosen N (2021). Regulation of PTEN translation by PI3K signaling maintains pathway homeostasis. Mol. Cell 81, 708–723.e5. [PubMed: 33606974]

Na J, Chen Q, and Ren X (2018). Saturation Dynamics and Modeling. In Adaptive Identification and Control of Uncertain Systems with Non-smooth Dynamics (Academic Press), pp. 195–201.

Nakakuki T, Birtwistle MR, Saeki Y, Yumoto N, Ide K, Nagashima T, Brusch L, Ogunnaike BA, Okada-Hatakeyama M, and Kholodenko BN (2010). Ligand-specific c-Fos expression emerges

Author Manuscript Author Manuscript Author Manuscript Author Manuscript

from the spatiotemporal control of ErbB network dynamics. Cell 141, 884–896. [PubMed: 20493519]

Nguyen LK, and Kholodenko BN (2016). Feedback regulation in cell signalling: lessons for cancer therapeutics. Semin. Cell Dev. Biol 50, 85–94. [PubMed: 26481970]

Niederst MJ, and Engelman JA (2013). Bypass mechanisms of resistance to receptor tyrosine kinase inhibition in lung cancer. Sci. Signal 6, re6. [PubMed: 24065147]

Nikolaou M, Pavlopoulou A, Georgakilas AG, and Kyrodimos E (2018). The challenge of drug resistance in cancer treatment: a current overview. Clin. Exp. Metastasis 35, 309–318. [PubMed: 29799080]

Pao W, Miller VA, Politi KA, Riely GJ, Somwar R, Zakowski MF, Kris MG, and Varmus H (2005). Acquired resistance of lung adenocarcinomas to gefitinib or erlotinib is associated with a second mutation in the EGFR kinase domain. PLoS Med. 2, e73. [PubMed: 15737014]

Poulikakos PI, Zhang C, Bollag G, Shokat KM, and Rosen N (2010). RAF inhibitors transactivate RAF dimers and ERK signalling in cells with wild-type BRAF. Nature 464, 427–430. [PubMed: 20179705]

Prahallad A, Sun C, Huang S, Di Nicolantonio F, Salazar R, Zecchin D, Beijersbergen RL, Bardelli A, and Bernards R (2012). Unresponsiveness of colon cancer to BRAF(V600E) inhibition through feedback activation of EGFR. Nature 483, 100–103. [PubMed: 22281684]

Qiao L, Nachbar RB, Kevrekidis IG, and Shvartsman SY (2007). Bistability and oscillations in the Huang-Ferrell model of MAPK signaling. PLoS Comput. Biol 3, 1819–1826. [PubMed: 17907797]

Rauch N, Rukhlenko OS, Kolch W, and Kholodenko BN (2016). MAPK kinase signalling dynamics regulate cell fate decisions and drug resistance. Curr. Opin. Struct. Biol 41, 151–158. [PubMed: 27521656]

Ritt DA, Monson DM, Specht SI, and Morrison DK (2010). Impact of feedback phosphorylation and Raf heterodimerization on normal and mutant B-Raf signaling. Mol. Cell. Biol 30, 806–819. [PubMed: 19933846]

Romano D, Nguyen L, Matallanas D, Halasz M, Doherty C, Kholodenko BN, and Kolch W (2014). Protein interaction switches coordinate Raf-1 and MST2/Hippo signalling. Nat Cell Biol 16, 673–684. 10.1038/ncb2986. [PubMed: 24929361]

Rukhlenko OS, Khorsand F, Krstic A, Rozanc J, Alexopoulos LG, Rauch N, Erickson KE, Hlavacek WS, Posner RG, Gómez-Coca S, et al. (2018). Dissecting RAF Inhibitor Resistance by Structure-based Modeling Reveals Ways to Overcome Oncogenic RAS Signaling. Cell Syst. 7, 161–179.e14. [PubMed: 30007540]

Rushworth LK, Hindley AD, O'Neill E, and Kolch W (2006). Regulation and role of Raf-1/B-Raf heterodimerization. Mol. Cell. Biol 26, 2262–2272. [PubMed: 16508002]

Ryan MB, Fece de la Cruz F, Phat S, Myers DT, Wong E, Shahzade HA, Hong CB, and Corcoran RB (2020). Vertical Pathway Inhibition Overcomes Adaptive Feedback Resistance to $KRAS^{G12C}$ Inhibition. Clin. Cancer Res 26, 1633–1643. [PubMed: 31776128]

Santra T, Rukhlenko O, Zhernovkov V, and Kholodenko BN (2018). Reconstructing static and dynamic models of signaling pathways using Modular Response Analysis. Curr. Opin. Syst. Biol 9, 11–21.

Schindelin J, Arganda-Carreras I, Frise E, Kaynig V, Longair M, Pietzsch T, Preibisch S, Rueden C, Saalfeld S, Schmid B, et al. (2012). Fiji: an open-source platform for biological-image analysis. Nat. Methods 9, 676–682. [PubMed: 22743772]

Segatto O, Anastasi S, and Alemà S (2011). Regulation of epidermal growth factor receptor signalling by inducible feedback inhibitors. J. Cell Sci 124, 1785–1793. [PubMed: 21576352]

Sturm OE, Orton R, Grindlay J, Birtwistle M, Vyshemirsky V, Gilbert D, Calder M, Pitt A, Kholodenko B, and Kolch W (2010). The mammalian MAPK/ERK pathway exhibits properties of a negative feedback amplifier. Sci. Signal 3, ra90. [PubMed: 21177493]

Sun C, and Bernards R (2014). Feedback and redundancy in receptor tyrosine kinase signaling: relevance to cancer therapies. Trends Biochem. Sci 39, 465–474. [PubMed: 25239057]

Author Manuscript Author Manuscript Author Manuscript Author Manuscript

Sun C, Wang L, Huang S, Heynen GJ, Prahallad A, Robert C, Haanen J, Blank C, Wesseling J, Willems SM, et al. (2014). Reversible and adaptive resistance to BRAF(V600E) inhibition in melanoma. Nature 508, 118–122. [PubMed: 24670642]

Thomaseth C, Fey D, Santra T, Rukhlenko OS, Radde NE, and Kholodenko BN (2018). Impact of measurement noise, experimental design, and estimation methods on Modular Response Analysis based network reconstruction. Sci. Rep 8, 16217. [PubMed: 30385767]

Tsyganov MA, Kolch W, and Kholodenko BN (2012). The topology design principles that determine the spatiotemporal dynamics of G-protein cascades. Mol. Biosyst 8, 730–743. [PubMed: 22218529]

Tyson JJ, and Othmer HG (1978). The dynamics of feedback control circuits in biochemical pathways. Progr. Theor. Biol 5, 1–62.

Van Cutsem E, Huijberts S, Grothey A, Yaeger R, Cuyle PJ, Elez E, Fakih M, Montagut C, Peeters M, Yoshino T, et al. (2019). Binimetinib, Encorafenib, and Cetuximab Triplet Therapy for Patients With *BRAF* V600E-Mutant Metastatic Colorectal Cancer: Safety Lead-In Results From the Phase III BEACON Colorectal Cancer Study. J. Clin. Oncol 37, 1460–1469. [PubMed: 30892987]

Varga A, Ehrenreiter K, Aschenbrenner B, Kocieniewski P, Kochanczyk M, Lipniacki T, and Baccarini M (2017). RAF1/BRAF dimerization integrates the signal from RAS to ERK and ROKα. Sci. Signal 10, eaai8482. [PubMed: 28270557]

Ventura JJ, Hübner A, Zhang C, Flavell RA, Shokat KM, and Davis RJ (2006). Chemical genetic analysis of the time course of signal transduction by JNK. Mol. Cell 21, 701–710. [PubMed: 16507367]

Volinsky N, and Kholodenko BN (2013). Complexity of receptor tyrosine kinase signal processing. Cold Spring Harb. Perspect. Biol 5, a009043. [PubMed: 23906711]

Wang L, Perera BG, Hari SB, Bhhatarai B, Backes BJ, Seeliger MA, Schürer SC, Oakes SA, Papa FR, and Maly DJ (2012). Divergent allosteric control of the IRE1α endoribonuclease using kinase inhibitors. Nat. Chem. Biol 8, 982–989. [PubMed: 23086298]

Weinstein IB, and Joe A (2008). Oncogene addiction. Cancer Res. 68, 3077–3080. [PubMed: 18451130]

Widmann C, Gibson S, Jarpe MB, and Johnson GL (1999). Mitogen-activated protein kinase: conservation of a three-kinase module from yeast to human. Physiol. Rev 79, 143–180. [PubMed: 9922370]

Wong ES, Fong CW, Lim J, Yusoff P, Low BC, Langdon WY, and Guy GR (2002). Sprouty2 attenuates epidermal growth factor receptor ubiquitylation and endocytosis, and consequently enhances Ras/ERK signalling. EMBO J. 21, 4796–4808. [PubMed: 12234920]

Yaeger R, and Corcoran RB (2019). Targeting Alterations in the RAF-MEK Pathway. Cancer Discov. 9, 329–341. [PubMed: 30770389]

Yalamanchili N, Zak DE, Ogunnaike BA, Schwaber JS, Kriete A, and Kholodenko BN (2006). Quantifying gene network connectivity in silico: scalability and accuracy of a modular approach. Syst. Biol. (Stevenage) 153, 236–246. [PubMed: 16986625]

Yeh PJ, Hegreness MJ, Aiden AP, and Kishony R (2009). Drug interactions and the evolution of antibiotic resistance. Nat. Rev. Microbiol 7, 460–466. [PubMed: 19444248]

Yen I, Shanahan F, Merchant M, Orr C, Hunsaker T, Durk M, La H, Zhang X, Martin SE, Lin E, et al. (2018). Pharmacological Induction of RAS-GTP Confers RAF Inhibitor Sensitivity in KRAS Mutant Tumors. Cancer Cell 34, 611–625.e7. [PubMed: 30300582]

Yi TM, Huang Y, Simon MI, and Doyle J (2000). Robust perfect adaptation in bacterial chemotaxis through integral feedback control. Proc. Natl. Acad. Sci. USA 97, 4649–4653. [PubMed: 10781070]

Yuan X, Tang Z, Du R, Yao Z, Cheung SH, Zhang X, Wei J, Zhao Y, Du Y, Liu Y, et al. (2020). RAF dimer inhibition enhances the antitumor activity of MEK inhibitors in K-RAS mutant tumors. Mol. Oncol 14, 1833–1849. [PubMed: 32336014]

Zañudo JGT, Steinway SN, and Albert R (2018). Discrete dynamic network modeling of oncogenic signaling: mechanistic insights for personalized treatment of cancer. Curr. Opin. Syst. Biol 9, 1–10. [PubMed: 32954058]

Author Manuscript Author Manuscript Author Manuscript Author Manuscript

Highlights

- Feedback loops cannot fully buffer drug perturbations and recover signaling output
- Activating and inhibitory paths from a drug target can reactivate signaling output
- Drug target dimerization combined with feedback can restore signaling output
- Combining type I½ and II RAF inhibitors quells ERK reactivation in NRAS mutant cancers

Author Manuscript Author Manuscript Author Manuscript Author Manuscript

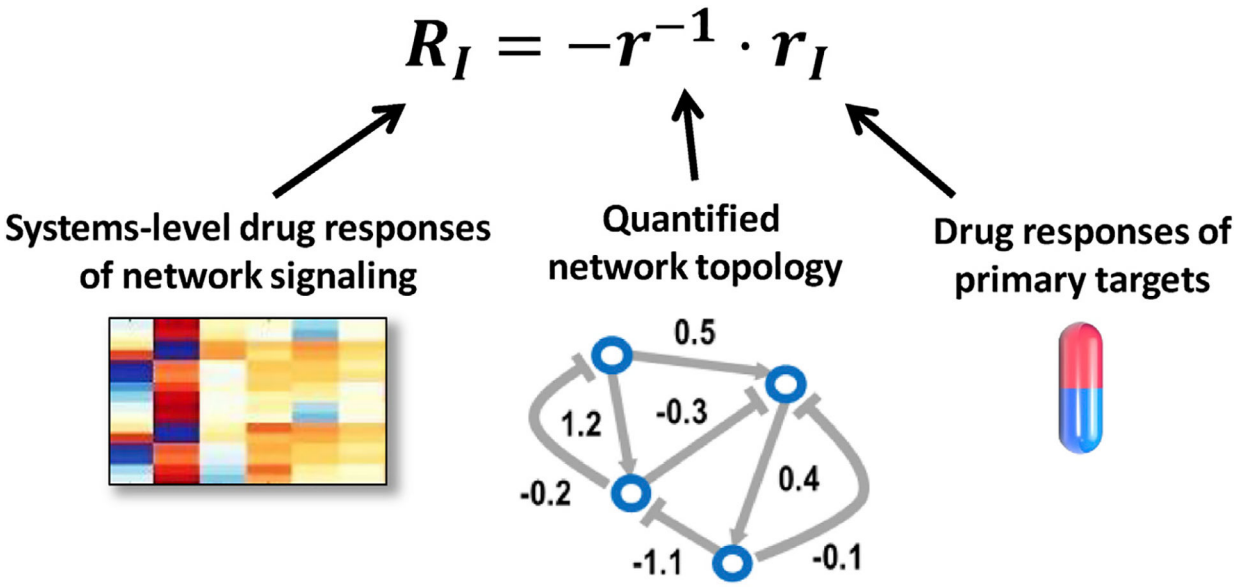

Figure 1. Systems-level drug responses are determined by MRA-quantified network connections and local drug responses of primary targets

Modular response analysis (MRA) allows the calculation of the systems-level network responses R_I to different drugs (I). R_I is vector of systems-level responses; the matrix r is the connection matrix that quantifies network topology by giving the directions, signs, and magnitudes of network connection strengths; and the vector r_I quantifies the local responses of primary targets to a drug. MRA demonstrates that paradoxical activation by a drug can only be observed because of a specific network topology (the term r^{-1}) or if this drug cannot inhibit its primary targets (the term r_I).

Author Manuscript Author Manuscript Author Manuscript Author Manuscript

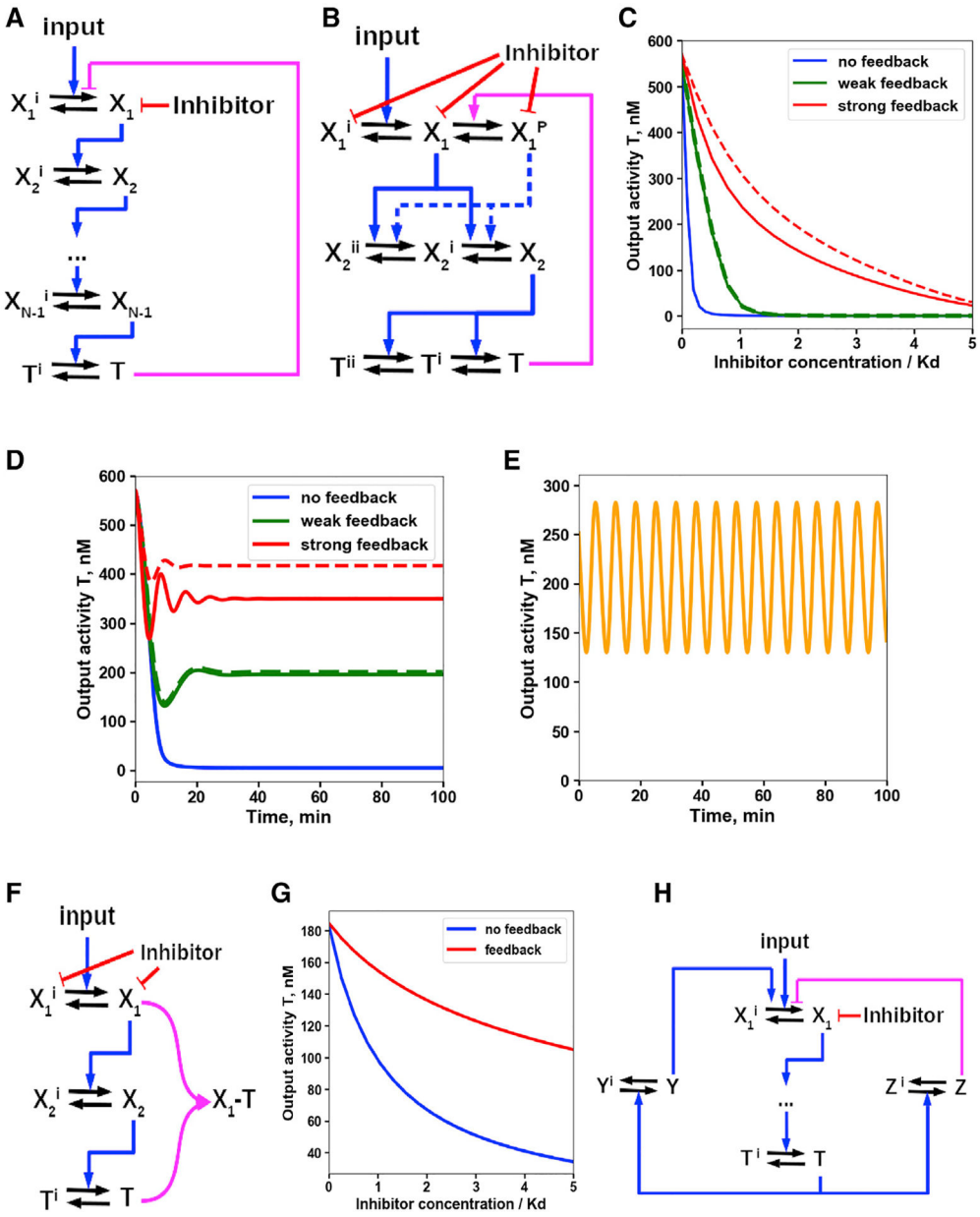

Figure 2. Kinetic schemes and dose responses of signaling pathways with feedback loops

(A) Activating kinase cascade with negative feedback from the pathway output protein (T^i is an inactive form and T is an active form) to the first-tier kinase (X_1). Inhibitor (I) can bind to an active form(X_1) and/or an inactive (X_1^i) form of this kinase that is the primary drug target.

(B) Schematic of a mass-action, mechanistic model of a 3-tier cascade with negative feedback mediated by the inhibitory phosphorylation of X_1 by T. Drug I can bind to inactive (X_1^i), active (X_1), and feedback-modified (X_1^P) kinase forms.

(C) Steady-state dependence of T on the drug concentration I (dose responses). The inhibitor dose is normalized by K_d. Solid red, green, and blue lines correspond to strong feedback, weak feedback, or no feedback. Dashed red and green lines correspond to the reduced

Author Manuscript Author Manuscript Author Manuscript Author Manuscript

affinities of the feedback-modified kinase form X_1^P for the drug. The input signal was adjusted to obtain the same initial output activity at different feedback strengths.

(D) The time course of T in response to the drug dose equal to 0.5 K_d for different strengths of negative feedback.

(E) Oscillations occur when negative feedback is too strong.

(F) Negative feedback is mediated by the formation of an inactive complex between X_1 by T rather than by inhibitory modification of X_1. The inhibitor I binds to both active (X_1) and inactive forms X_1^i.

(G) Dose responses for negative feedback mediated by protein sequestration (red) and in the absence of feedback (blue). See STAR Methods for details.

(H) Kinetic scheme of a cascade with negative and positive feedback loops from the output protein to the upstream activator that is a primary drug target.

Author Manuscript Author Manuscript Author Manuscript Author Manuscript

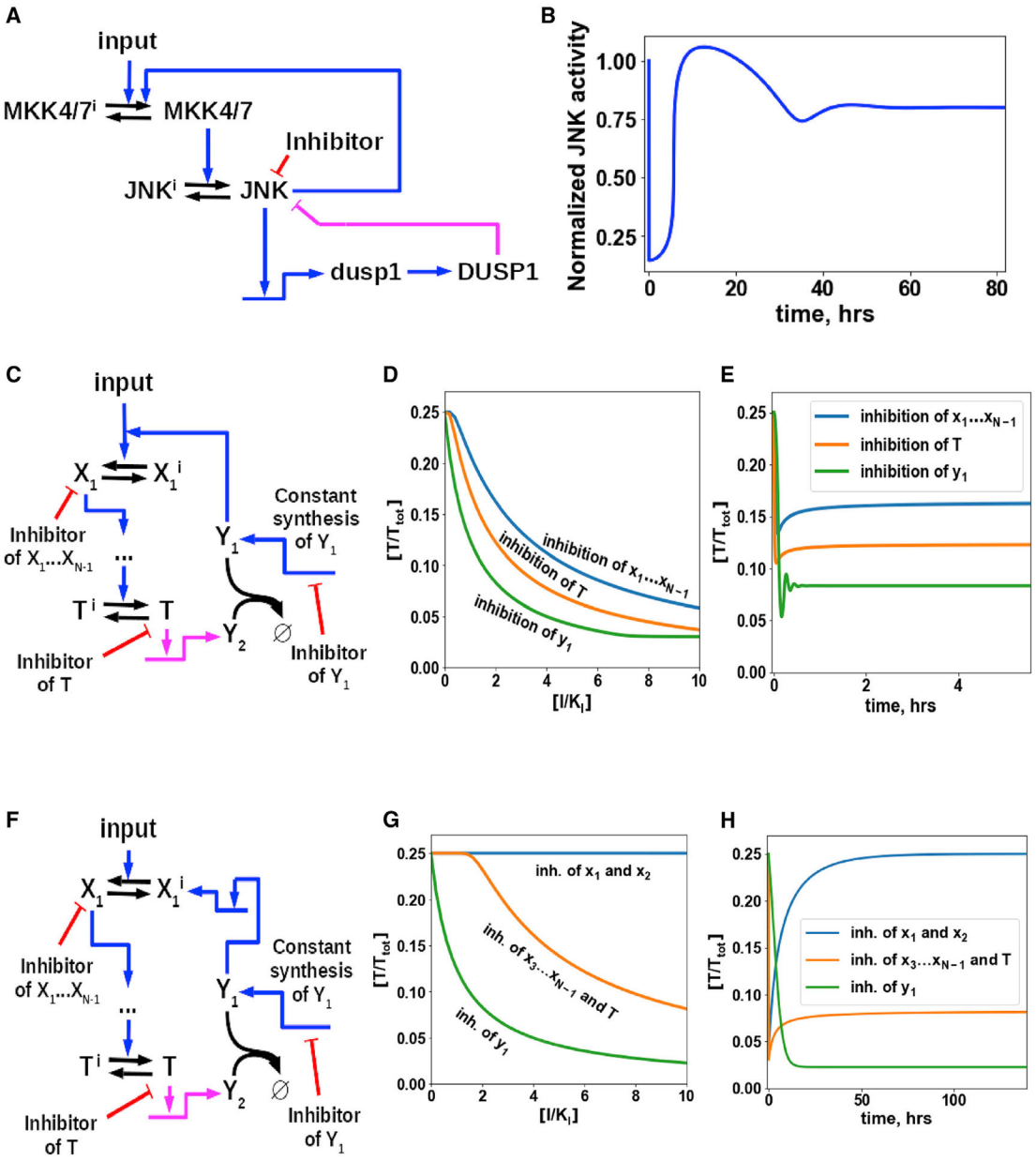

Figure 3. Transcriptional feedback loops and weak spots of the integral control in cell signaling

(A) A diagram of the JNK signaling pathway featuring negative transcriptional and positive phosphorylation feedbacks.

(B) Time course of the JNK activity response to JNK inhibition. A transient, prolonged period of reactivation and overshoot of the JNK activity occurs because of the delay in the negative feedback circuit of DUSP1 expression.

(C) A signaling pathway that includes an integral control module consisting of two species Y_1 and Y_2, where Y_1 activates the conversion of an inactive form X_1^i to active form (X_1). Designations are the same as in Figure 2.

(D and E) Dose response (D) and time courses (E) of the output activity T show the lack of complete reactivation for this pathway.

Author Manuscript Author Manuscript Author Manuscript Author Manuscript

(F) A signaling pathway with an integral control module where Y_1 catalyzes the synthesis of the inactive kinase form, X_1^i.

(G and H) Dose responses (G) and time courses (H) of T to drug inhibition of X_1 and X_2 (blue lines), the kinases downstream of X_2, including output T (orange), or the species in the control module (green). See STAR Methods for equations and parameters.

Author Manuscript Author Manuscript Author Manuscript Author Manuscript

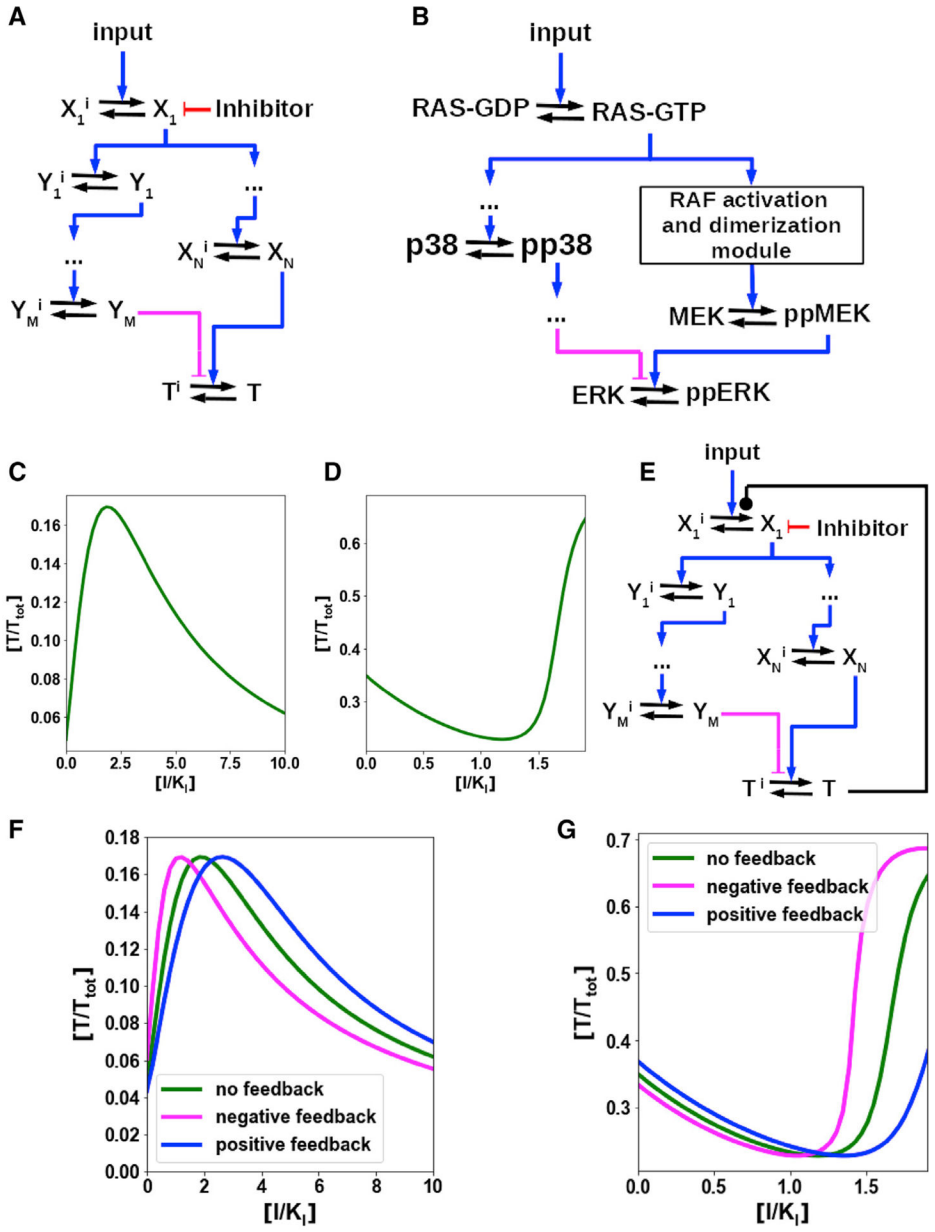

Figure 4. Two feedforward connections, positive and negative, can lead to complete signaling reactivation

(A) Kinase X_1, which is a primary drug target, activates the output T through pathway X and also activates pathway Y that inhibits T.

(B) Negative feedforward connection from RAS to ERK is mediated by the p38 pathway.

(C and D) Dose responses show different modes of paradoxical activation of the output T by an inhibitor (I). The negative (C) or positive (D) feedforward dominates. The output activity is normalized by its activity in the drug absence, and doses are normalized by the drug K_d.

(E) The output T feeds back to the kinase at the crosstalk point, which is the primary drug target. Feedback can be positive or negative.

(F and G) Dose responses are modulated by feedback. Negative feedback (magenta) narrows, whereas positive feedback (blue) expands the range of drug doses where signaling

is paradoxically activated by pathway crosstalk. Green curves, no feedback (STAR Methods).

Author Manuscript Author Manuscript Author Manuscript Author Manuscript

Author Manuscript Author Manuscript Author Manuscript Author Manuscript

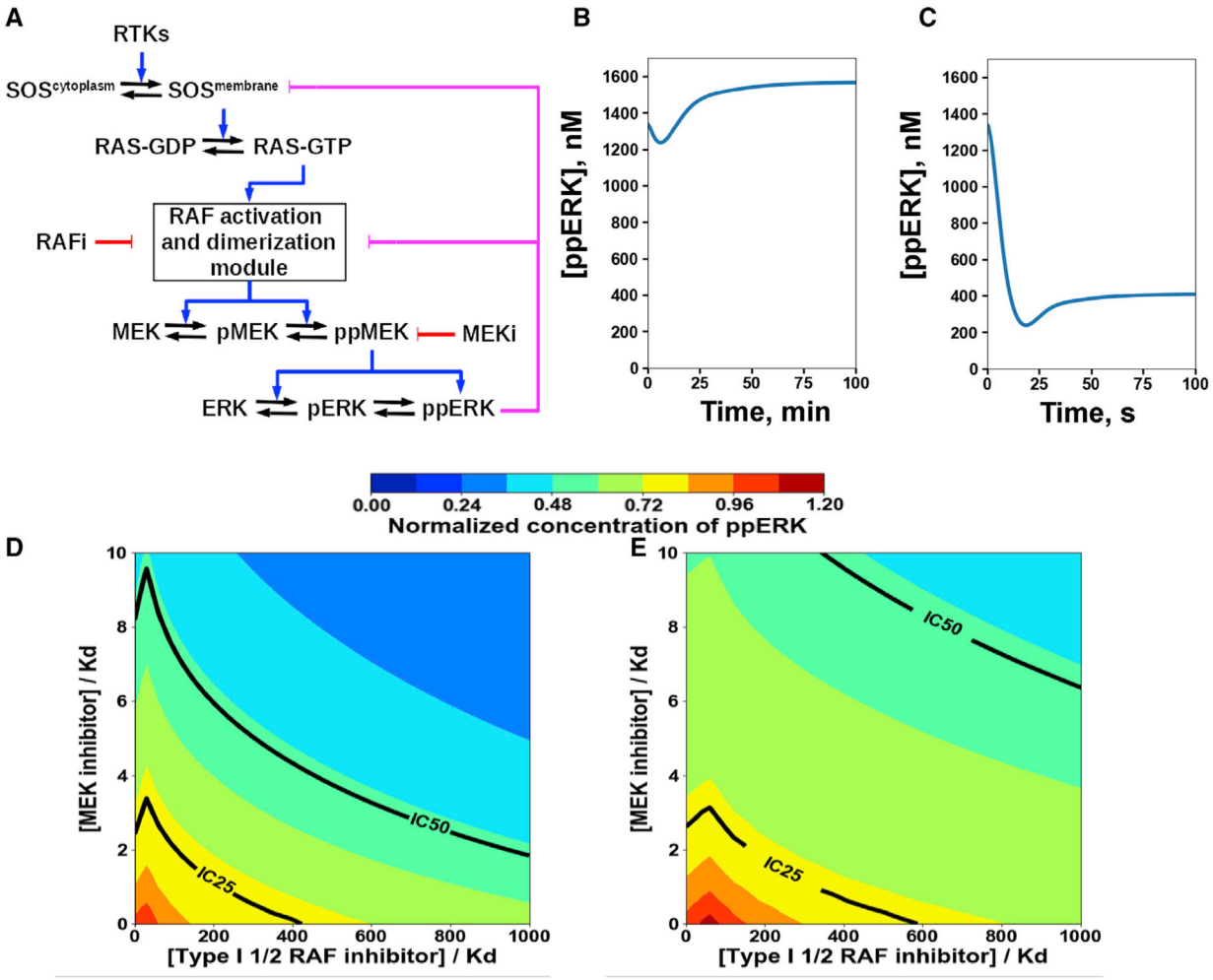

Figure 5. A negative feedback loop from ERK to SOS facilitates ERK paradoxical activation by RAF inhibitors

(A) A diagram of a structure-based dynamic model of the ERK pathway featuring negative feedback loops from ERK to RAF and SOS (see STAR Methods).

(B and C) Time courses of the ERK activity responses to RAF inhibitors, which induce (B) or do not induce (C) RAF dimerization.

(D and E) Steady-state ERK signaling responses to type I½ RAF and MEK inhibitors and their combinations are analyzed using Loewe isoboles. IC_{25} and IC_{50} lines correspond to the drug doses that achieve 25% or 50% ERK inhibition, respectively. In cells with a $BRAF^{V600E}$ mutation and WT RAS synergy between type I½ RAF and MEK inhibitors is observed at wider dose ranges for (D) low (~25 nM RAS-GTP of 750 nM total RAS) than (E) high WT RAS activities (~100 nM RAS-GTP of 750 nM total RAS).

Author Manuscript Author Manuscript Author Manuscript Author Manuscript

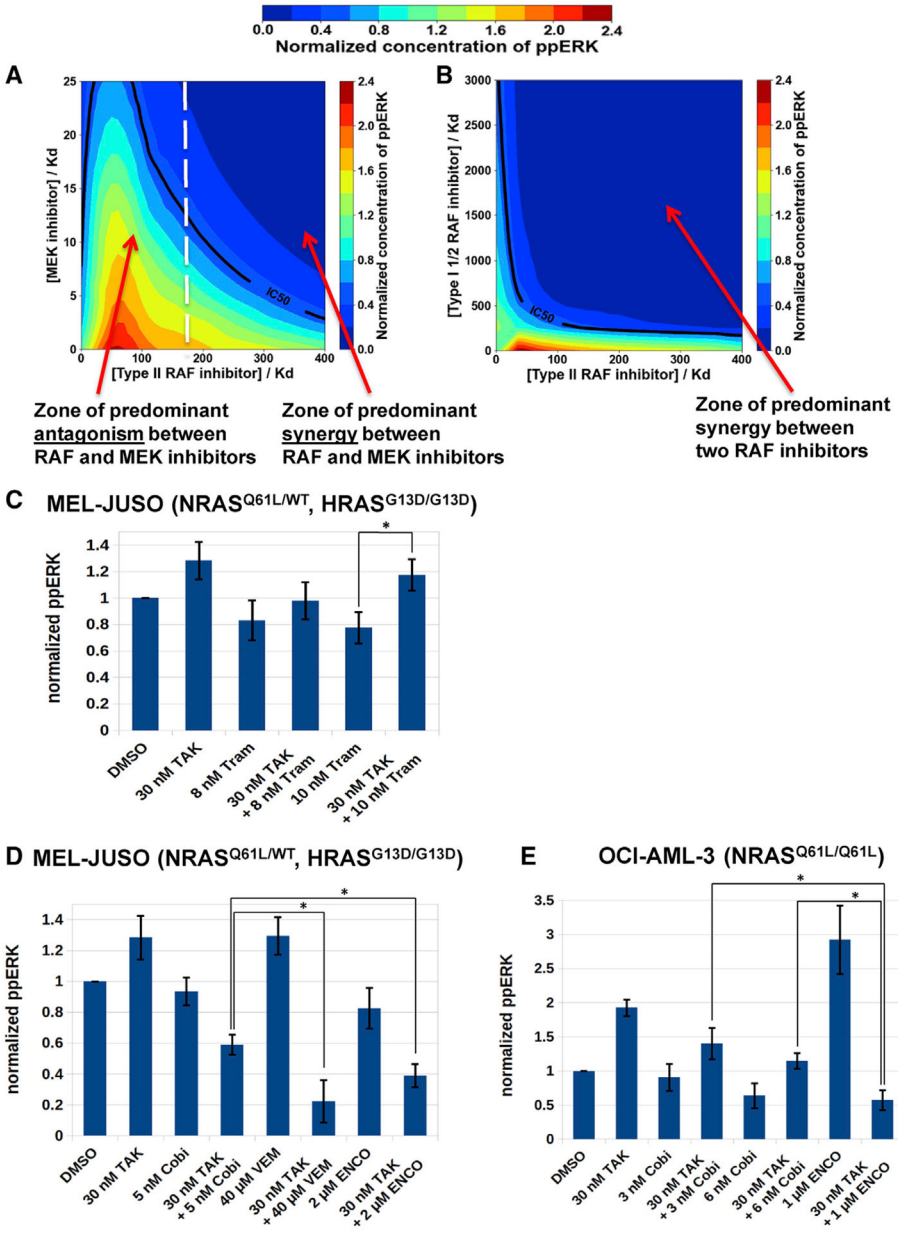

Figure 6. A combination of type I½ and type II RAF inhibitors efficiently suppresses reactivation of the ERK pathway in mutant RAS cells

(A and B) Calculated Loewe isoboles of ERK signaling responses to combinations (A) of MEK and type II RAF inhibitors and (B) type I½ and type II RAF inhibitors for cells with mutant RAS (~250 nM RAS-GTP) and WT RAF.

(C) ERK signaling responses to the MEK inhibitor trametinib and its combination with 30 nM type II RAF inhibitor TAK-632 measured in growing MEL-JUSO cells ($NRAS^{Q61L/WT}$, $HRAS^{G13D/G13D}$).

(D and E) Combinations of type I½ RAF inhibitor (vemurafenib or encorafenib) and type II RAF inhibitor (TAK-632) suppress ERK signaling more effectively than a combination of the MEK inhibitor cobimetinib with TAK-632 in growing (D) MEL-JUSO ($NRAS^{Q61L/WT}$, $HRAS^{G13D/G13D}$) and (E) OCI-AML-3 ($NRAS^{Q61l/Q61L}$) cells.

Signaling responses (C–E) are measured by western blots and quantified using ImageJ. Error bars show standard errors of the mean for 3 biological replicates. The asterisk indicates $p < 0.05$ calculated using unpaired t test.

Author Manuscript Author Manuscript Author Manuscript Author Manuscript

Author Manuscript Author Manuscript Author Manuscript Author Manuscript

KEY RESOURCES TABLE

REAGENT or RESOURCE	SOURCE	IDENTIFIER
Antibodies		
Anti-MAP Kinase (ERK-1, ERK-2) antibody produced in rabbit	Sigma-Aldrich	Cat. No. M5670; RRID: AB_477216
Monoclonal Anti-MAP Kinase, Activated (Diphosphorylated ERK-1&2) antibody produced in mouse	Sigma-Aldrich	Cat. No. M8159; RRID: AB_477245
Anti-rabbit IgG, HRP-linked Antibody	Cell Signaling Technologies	Cat. No. 7074; RRID: AB_2099233
Anti-mouse IgG, HRP-linked Antibody	Cell Signaling Technologies	Cat. No. 7076; RRID: AB_330924
Critical commercial assays		
Phospho(Thr202/Tyr204; Thr185/Tyr187)/Total ERK1/2 Assay Whole Cell Lysate Kit	MesoScale Discovery	K15107D
Pierce BCA Protein Assay Kit	ThermoFisher Scientific/Pierce	Cat. No. 23225
Chemicals, peptides, and recombinant proteins		
Vemurafenib (PLX4032)	Selleckchem	Cat. No. S1267
Cobimetinib	Selleckchem	Cat. No. S8041
TAK-632	Selleckchem	Cat. No.S7291
Trametinib	Selleckchem	Cat. No. S2673
Encorafenib (LGX818)	Selleckchem	Cat. No. S7108
Experimental models: Cell lines		
MEL-JUSO	DSMZ	ACC 74; RRID: CVCL_1403
OCI-AML-3	Gift from Prof. Ken Mills, Queen's University Belfast	RRID: CVCL_1844
Software and algorithms		
Python	N/A	N/A
Sage	(The Sage)	N/A
SciPy	N/A	N/A
MatplotLib	N/A	N/A
BioNetGen	Borisov et al., 2008; Chylek et al., 2014	N/A
Model codes in SBML format	This study	Data S1, S2, and S5